Check for updates

Towards cost-efficient and stable perovskite solar cells and modules: utilization of self-assembled monolayers

Haoliang Cheng, [ID] [a] Yungui Li [b] and Yufei Zhong [ID] *[ac]

Perovskite solar cells (PSCs) have attracted extensive attention in recent years due to their advantages such as low cost and flexibility. However, the serious charge recombination at the interface of the perovskite film and charge transport layers limit further improvement of the device performance to date. Thus, among the many methodologies to solve these issues, self-assembled monolayers (SAMs) are potential candidates due to their successful application in efficient PSCs. Accordingly, in this review, we introduce the recent progress of SAMs that have been extensively used as interfacial layers in PSCs and modules, with the aim to understand how to reduce the energy loss in PSCs by modulating the interfacial molecular interactions. According to the recent literature, we discuss the roles of the functional parts in SAMs and highlight the future design challenges/principles of SAMs. Finally, we emphasize that together with other strategies for interfacial modification, SAMs can push PSCs into future practical application, realizing cost-efficient and stable processing.

1. Introduction

Presently, considering global warming and the energy crisis, the development of new sustainable energy sources has become urgent and attractive. In this case, photovoltaics (PVs) can cost-efficiently convert solar energy into electricity, which is ideal technology for the future society. Among the PV technologies, perovskite solar cells (PSCs) have emerged as promising candidates, the origin of which dates back to the pioneering work of Miyasaka in 2009,[1] where a perovskite absorber was firstly used to sensitize a mesoporous TiO_2 film with liquid electrolyte. However, these liquid-based devices exhibited poor stability with a power conversion efficiency (PCE) of 3.8%. Subsequently, Park and co-authors[2] reported the use of Spiro-OMeTAD as a hole transporting layer to replace the liquid electrolyte for solid-state PSCs, realizing an increase in the PCE to 9.7%. Snaith and co-authors[3] reported mixing Cl in I-based perovskite to suppress its dissolution, consequently improving the PCE to 10.9%. Due to this rapid development, PSCs have become a "game changer" in the field of PVs, with a PCE of over 25% achieved for single-junction devices to date, which is very close to that of single silicon-based devices.[4,5]

Nevertheless, PSCs still suffer from the presence of defects in the bulk and surface of the perovskite film, particularly those in the surface, which lead to sub-optimal contact for charge transfer at the electrode/perovskite interface. Additionally, these defects induce serious charge recombination and instability. Therefore, the low film quality and energy level mismatch between the perovskite absorber and charge transport layer limits the PCE of PSCs.[6–9]

Many methods have been developed to address the above-mentioned issues, such as doping and surface treatment.[10] Among the various methods, the use of SAMs is cost efficient with wide modulation possibilities. SAMs with anchoring groups can chemically adsorb on the conductive substrate or metal oxide-based charge transport layers, which can induce a dipole moment at the interface, and then shift the work function. Moreover, the terminal group of SAMs can interact with the perovskite and improve the quality of the film, reducing the amount of defects at the interface.[11] Thus, SAM-based interfacial materials with multifunctional groups can be regarded as promising candidates for solving the issues associated with PSCs.

In this review, we aim to introduce the recent progress in self-assembled monolayers (SAMs) that have been extensively used as interfacial layers in perovskite solar cells (PSCs) and modules. Firstly, the concept and methods for the deposition of SAMs are introduced. Subsequently, the applications of SAMs in PSCs are divided into three parts, as follows: (i) as hole transport layers (or interfacial modification layers) in PSCs;

[a] School of Materials Science and Engineering, NingboTech University, No. 1 South Qianhu Road, Ningbo, P. R. China. E-mail: yufei.zhong@nit.zju.edu.cn

[b] Max Planck Institute for Polymer Research, Ackermannweg 10, 55128 Mainz, Germany

[c] Ningbo Innovation Center, Zhejiang University, No. 1 South Qianhu Road, Ningbo, P. R. China

This journal is © The Royal Society of Chemistry and the Chinese Chemical Society 2023

(ii) as electron transport layers (or interfacial modification layers for metal oxide) in PSCs; and (iii) SAMs for large-area perovskite modules. Additionally, the relationship between the properties of SAMs and the performance of PSCs is discussed in detail, such as the role of the anchoring groups, linker, and the head part of SAMs. After summarizing the concepts of SAMs and their application in PSCs, the mechanism for SAMs improving the performance of PSCs will be discussed. Subsequently, we provide some guidelines for the further strategy of designing molecules. Eventually, the conclusions and challenges associated with SAMs in PSCs are summarized.

2. Perovskite solar cells

The perovskite absorber possesses an ABX_3 structure, where A is an organic (MA = $CH_3NH_3^+$, FA = $CH(NH_2)_2^+$) or inorganic cation (Cs^+, Rb^+); B is a metal ion (Pb^{2+}, Sn^{2+}); and X is a halide anion.[12] The beneficial properties of the perovskite absorber endow PSCs with a high performance, such as high absorption coefficient, long carrier lifetime, high trap tolerance, high dielectric constant, and tunable bandgap.

Two general device structures are used in PSCs, namely, mesoporous and planar structures. The former is referred to as mesoporous TiO_2-based devices, which are derived from dye-sensitized solar cells.[13] In this structure, the mesoporous TiO_2 is the electron transport layer (ETL) and Spiro-OMeTAD is the hole transport layer (HTL).[14,15] In the case of the latter, it contains n–i–p (regular)- and p–i–n (inverted)-structured devices. In the n–i–p structure, the ETL is deposited on the surface of a transparent conductive glass substrate (TCO) and the HTL is deposited on the top of a perovskite film. Alternatively, in the p–i–n structure, the position of the ELT and HTL is the reverse.[16]

3. Concept and deposition method of SAMs

3.1 Concept of SAMs

SAMs are defined as one or a few layers of molecules with functional groups, which are naturally formed atop a solid substrate.[17,18] The self-assembly of molecules on the surface of a substrate is a thermodynamically favorable process.[19] Typically, SAMs are vertically aligned on the surface of the substrate with certain angle relative to the surface normal. SAMs usually contain three parts,[20,21] including anchoring, linker, and terminal groups, as shown in Fig. 1.

(1) Anchoring group: the role of the anchoring group is to induce interactions between the SAM molecules and the substrate. In this case, different anchoring groups (–COOH, –PO_3H, –SO_3H, –SH, –SiOR, *etc.*) can bind to specific substrates (FTO, ITO, NiO, SnO_2, ZnO, and TiO_2), which affords many options for the preparation of electrodes and SAMs, respectively.

(2) Linker group: the linker group is the backbone of SAMs, which bridges the terminal and anchoring groups. The length of the backbone plays an important role in electronic
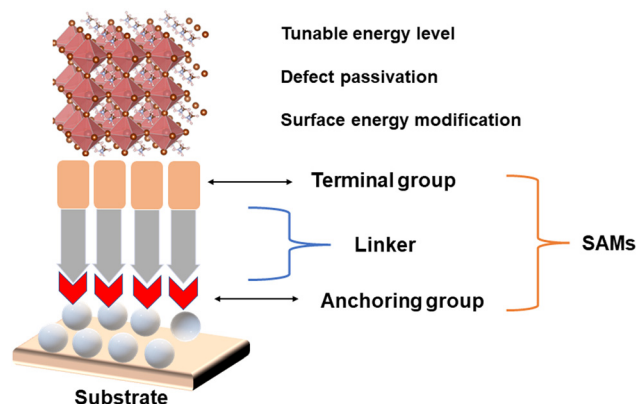

Fig. 1 Schematic diagram of SAMs with functional part inserted on the substrate and perovskite.

separation and building barrier layers. The linker group can be divided into non-conjugated (alkyl chain) and conjugated (aromatic ring) linkers, which can display various characteristics for charge transfer. Additionally, the linker group is responsible for the adjacent interaction between individual molecules in the process of self-assembly, which affects the final packing structure.

(3) Terminal group: the terminal group interacts with the overlayer or atmosphere. If the terminal group has a functional group that can interact with the perovskite film, the SAM can consequently influence the formation and morphology of the perovskite film. In addition, the terminal group can form a dipole moment to tune the energy level. Carbazole-based donors are widely used terminal groups. Energetically, the choice of terminal group is also important for adjusting the work function of the target surface.

3.2 Methods for the deposition of SAMs

The methods for the deposition of SAMs for application in PSCs can be divided into vapor-phase and liquid-phase deposition.[22]

3.2.1 Vapor-phase deposition. This process requires the activated surfaces of the conductive substrate to be exposed to an atmosphere filled with the vapor of organic molecules under high vacuum, which requires annealing to strengthen the bonding to the substrate.

Vapor-phase deposition has the advantages of not requiring a (liquid) solvent and the formed monolayers are more homogeneous than that with other methods. However, this process proceeds under high vacuum pressure, which is necessary to create the vapor phase, making it less cost-efficient and scalable.

3.2.2 Liquid-phase deposition. Liquid-phase methods involve dip- or spin-coating the SAM solution on the substrate. Dip-coating is a general method for mesoporous surfaces, which refers to the immersion of a conductive substrate in the SAM solution. The process of adsorption can be controlled by tuning the solvent component, solvent concentration, and dipping time. However, the dip-coating method, in most cases, requires a long time to deposit the SAM because of the slow process of adsorption. Alternatively,

spin-coating can be employed to rapidly fabricate a monolayer on a conductive substrate. Consequently, the dip-coating method is suitable for mesoporous metal oxide-based substrates, while the spinning-coating method is more popular for planar-structured substrates.

4. The mechanism of SAMs in improving the performance of PSCs

4.1 Energy-level alignment

Under illumination, the perovskite absorber can generate free charge carriers because of its low binding energy. The free charge carriers are collected by the electrode or charge transport layers. However, if the energy level between the CTL and perovskite is mismatched, serious charge recombination occurs. Due to the existence of dipole moments, SAMs can easily improve the energy level alignment between the perovskite and charge transport layer (CTL) or electrode, which facilitates electron or hole transfer. In addition, a shift in the work function (WF) can also occur under this condition, which benefits V_{oc} and/or charge injection. According to the WF theory, the direction and change in the dipole moment are related to the variation of the WF.[23] The relation between the change in work function ($\Delta\varphi$) and dipole moment can be expressed by the following equation:

$$\Delta\varphi = -N\left[\frac{\mu_{\perp SAM}}{\varepsilon_0 k_{SAM}} + \frac{\mu_{M-S}}{\varepsilon_0 K_{M-S}}\right] \qquad (1)$$

where N is the density of molecules anchored on the surface, k is the dielectric constant of the SAM layer, ε_0 is the permittivity of free space and $\mu_{\perp SAM}$ refers to the component of dipole moment normal to the surface.[24] According to eqn (1), if the dipole moment of the SAM is positive, the change in WF is negative. In the case of SAMs as HTLs, the dipole moment of SAMs should be positive to obtain a high voltage. However, for SAMs as ETLs, the dipole moments of the SAMs should be negative.

4.2 Passivation effect

There are abundant traps on the surface of the charge transport layers (especially metal oxides) and perovskite film. These defects can act as non-radiative recombination centers, decreasing the carrier density, charge carrier lifetime, and charge diffusion length, resulting in severe deterioration of the device performance. Accordingly, the bifunctional groups of SAMs can passivate the defects in the charge transport layers (especially metal oxides) and perovskite films (uncoordinated Pb^{2+}). In addition, they can adjust the morphology and improve the quality of the perovskite film. Consequently, these functions can not only improve the device figure of merit but also the long-term stability in most cases. After describing the mechanism of SAMs in improving the performance of PSCs, we present a detailed introduction about the recent progress of different categories of SAMs for PSCs in Section 5.

5. SAMs as hole transport layers or modifying layers for p−i−n-structured perovskite solar cells

5.1 SAMs as hole transport layers

5.1.1 Carbazole-based SAMs. In p–i–n-structured PSCs, the widely used HTLs are PEDOT:PSS, PTAA, and NiO_x. These HTLs have been employed to fabricate many efficient PSCs, but some major problems still hamper the further improvement in device performance. Among the HTLs, the instability and mismatched interfacial energy levels of PEDOT:PSS remain major challenges. In the case of PTAA-based polymers, the variation in molecular weight and wettability of the resulting film still have an adverse impact on the perovskite film formed atop them. Regarding NiO_x-based HTLs, their low hole mobility and electronic traps lead to devices with a low performance.[25–27] Considering the challenges associated with the HTLs in inverted PSCs, SAM-based HTLs can adjust the energy level, surface energy, and wettability of the substrate, providing an opportunity to address the main issues.[28]

Here, we briefly discuss the use of SAMs as HTLs for p–i–n-structured PSCs. Firstly, we introduce carbazole-based SAMs, which are the most widely used SAMs in PSCs, and their molecular structure is shown in Fig. 2. Magomedov et al.[29] reported the first SAMs as HTLs with carbazole-based phosphonic acid anchoring groups for PSCs. The mixed assembled V1036 with C4 achieved a PCE of 17.8% with a high FF (0.81), which is comparable to that of PTAA-based HTLs. Then, Al-Ashouri et al.[30] compared different carbazole derivative (V1036, MeO-2PACz and 2PACz)-based SAMs. Their results showed that 2PACz achieved a PCE of 20.9% with a V_{oc} of up to 1.19 V, which is higher than that of PTAA-based HTLs (19.2%). 2PACz displayed the closest alignment to the valence band maximum (VBM) of the perovskite, whereas V1036 showed the largest offset, which is consistent with the direction of their dipole moment. In addition, to further clarify the effect of band alignment on the buried interface between the HTL and perovskite film, they used photoluminescence (PL) and time-resolved PL for investigation. With an increase in the quasi Fermi level splitting (PTTA, V1036, MeO-2PACz, and 2PACz), the V_{oc} and PL lifetime improved. Consequently, the V_{oc} of 2PACz was the highest among the three SAMs because of its higher quasi Fermi level. Most SAMs are deposited through solution-processed methods. Alternatively, Farag et al.[31] developed a thermal evaporation method for the preparation of carbazole-based (2PACz, MeO-2PACz, and Me-4PACz) SAMs, which could realize near lossless energy at the interface and enhanced voltage. In addition, the method of vacuum deposition can improve perovskite wettability for unideal materials (Me-4PACz). The PCE of the evaporated Me-4PACz SAMs improved to 19.2%, which is comparable to that of solution-processed ideal materials (2PACz, 19.0%). Besides the above-mentioned applications in Pb-based PSCs, SAMs with carbazole-connected phosphonic acid anchoring groups also have a positive impact on tin-based PSCs.[32,33] Jen and
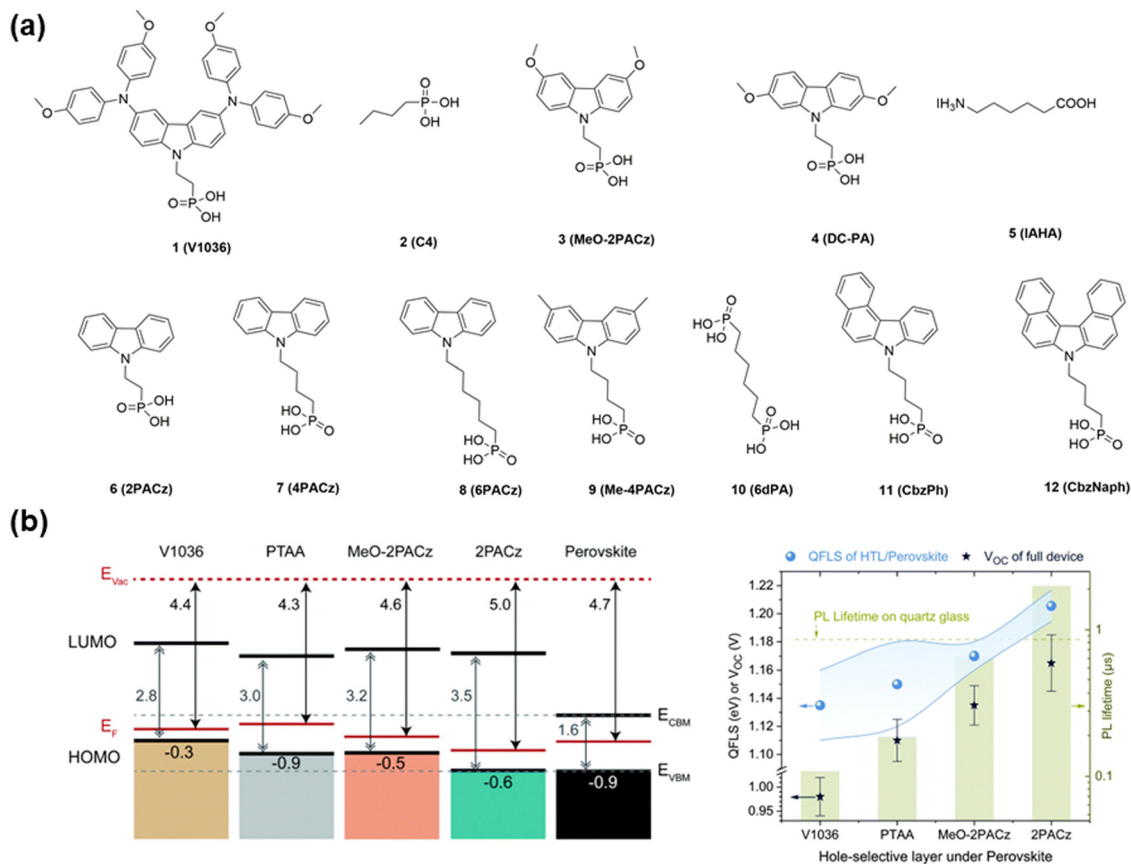
Fig. 2 (a) Molecular structure of carbazole derivative-based SAMs with phosphonic acid anchoring groups. (b) Energy level and photoluminescence analysis on perovskite with various SAMs as HTLs. Reproduced with permission.[30] Copyright 2019, The Royal Society of Chemistry.

co-authors[34] reported a strategy of co-assembly to combine SAMs with an ammonium passivator to construct efficient HTLs with reduced recombination loss. Additionally, the ammonium salt could adjust the surface energy and enhance the coverage of the SAMs. Finally, the modified device achieved a champion PCE of 23.59%. To further improve the performance of carbazole-based SAMs, they designed asymmetric and helical π-expansion, namely CbzPh and CbzNaph, respectively, as HTLs for inverted PSCs.[35] The larger molecular dipoles in CbzPh and CbzNaph could more efficiently tune the work function of ITO, whereas the stronger π–π interactions ensured a more ordered and denser molecular assembly. Thus, the PCE could be further improved to 24.1%. Although the PCEs of SAM-based devices have achieved good progress, the coverage of SAMs on a large area is still a challenge to overcome. To improve the wettability of Me-4PACz-treated surfaces, Magomedov and co-authors[36] introduced a second component (6dPA) in the precursor solution. The results showed that only a minority of the devices shunted because of low coverage, while the average PCE of 17.8% with an active area of 1 cm² was achieved. Luther and co-authors used the concept of co-deposition of SAMs with a perovskite layer to simplify the device and improve the performance. Me-4PACz was added to the perovskite precursor solution to improve the wettability of the perovskite solution on the ITO substrate, and consequently a PCE of 24.5% was achieved for the device.[37] Moreover, the

MeO-2PACz-based SAMs provided a suitable surface for growing perovskite single crystals for PSCs. Bakr and co-authors[38] reported the growth of mixed-cation perovskite single crystals on an MeO-2PACz-based HTL, which achieved a record PCE of 23.1% with enhanced operational stability for single-crystal PSCs. The above-mentioned results confirm that carbazole-based SAMs are good candidates as the interlayers in PSCs.

Although carbazole-based SAMs have achieved good performances in PSCs, the mechanism of charge transfer kinetics and trapping/de-trapping process are still not fully understood. Levine et al.[39] used transient surface photovoltage (SPV) to investigate the hole transfer rate and non-radiative recombination losses in different carbazole-based SAMs (Fig. 3(a)). The SPV measurements could monitor the variation in surface potential under photoexcitation and provide evidence about the type of injected charge (hole or electron).[40] The timescale of various dynamic processes for charge transfer and recombination is shown in Fig. 3(b). It was found that the transfer rate of holes to the ITO substrate is the fastest process with a timescale of 0.1–1 μs. In addition, the timescale for the recombination of holes and electrons is about 1 μs. Different chain lengths and head groups have a strong influence on the dipole moments and tunneling lengths for charge transfer. The resulting dipole moments affect the barrier heights between the energy level of the SAMs and the perovskite film. Me-4PACz and 2PACz
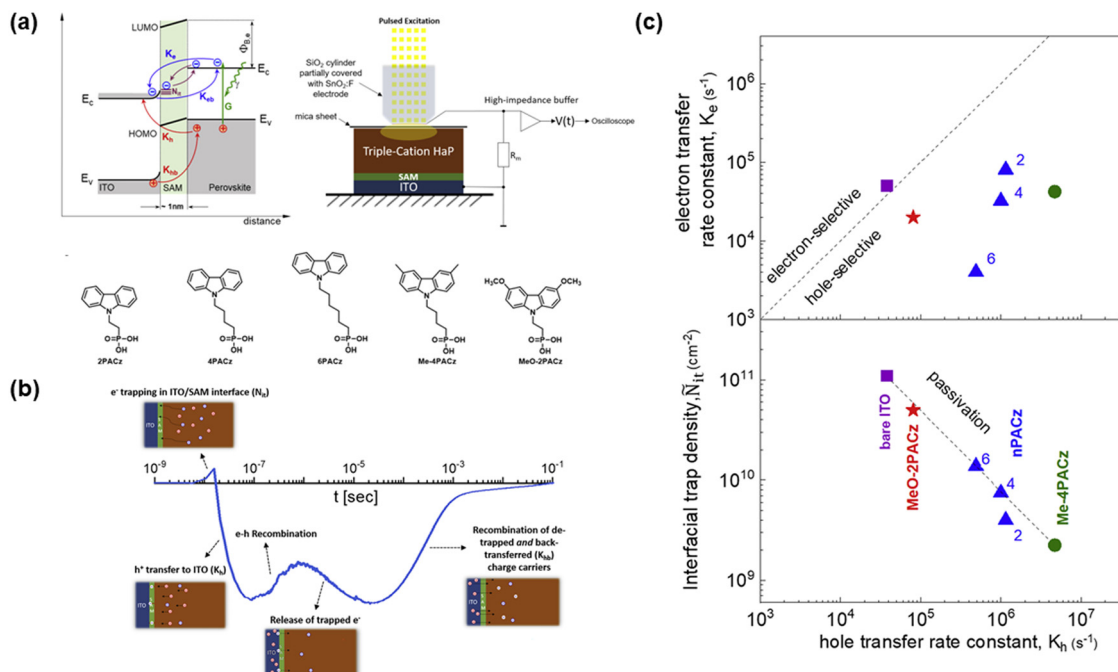

respectively. By varying the terminal group heteroatoms of the SAMs, they found that the Se-based SAM displayed the strongest interaction energy at the SAM/perovskite interface with a PCE of 22.73%, which benefited from the reduced interfacial trap density and enhanced charge-carrier lifetime.

To discuss the impact of SAMs on the work function of ITO, Singh *et al.*[42] systematically compared phenylphosphonic acid-based SAMs containing electron-donating or electron-withdrawing p-substituents on the surface of ITO. MxPPA (**16**), MyPPA (**17**) and PPA (**18**) have an electron-donating substituent and molecular dipole pointing away from the substrate surface, while CPPA (**19**) and NPPA (**20**) have an electron-withdrawing substituent and dipole pointing toward the surface. Consequently, the device with electron-withdrawing substituted SAMs (CPPA and NPPA) achieved a higher voltage. A similar observation was also reported by Li and co-authors,[43] who designed two D–A constructed SAMs (PPA: **21** and PPAOMe: **22**) with phosphonic acid as anchoring groups, which realized face-on π-stacking parallel to the conductive substrate. The electron-donating (–MeO) group (PPAOMe) decreased the oxidation potential. Consequently, the HOMO energy of PPA was lower than that of PPAOMe, which is beneficial for achieving a higher voltage. The PPA-based SAMs achieved a PCE of 23.24% with a V_{oc} of 1.14 V in a small area and about 20% for the perovskite module with an area of 17 cm^2. The operational stability of the PPA-based device also improved. According to the above-mentioned analysis of triphenylamine and phenothiazine derivative-based SAMs, it can be concluded that halogenated-substituted groups can adjust the energy level of SAMs to better match with the perovskite. In addition, the electron-withdrawing-substituted SAMs at the terminated group can induce the direction of the dipole moment to point toward the surface of the perovskite, which can contribute to a higher voltage. However, the presence of electron-donating-substituted SAMs in the terminal group will lead to the direction of the dipole moment pointing to the conductive substrate, and thus has an inverse effect on the photovoltage.

5.1.3 The effect of anchoring group on the performance of SAMs. The above-mentioned SAMs contained phosphonic acid

as their anchoring groups, which always affect their coverage, binding mode and strength on the conductive substrate. Li *et al.*[44] reported the preparation of SAMs with various anchoring groups (TPT-S6, TPT-C6 and TPT-P6) to investigate the effect of bonding strength on the monolayer quality, as shown in Fig. 5. Through the DFT calculation, it was found that –COOH and –SO$_3$H were favorably chemisorbed on the surface through dissociative chemisorption with O–H bond breaking (Fig. 5(a)). However, –PO$_3$H could be adsorbed *via* dissociative chemisorption or molecule adsorption. In addition, the more negative adsorption energy of phosphonic acid compared to sulfonate and carbonate indicated that –PO$_3$H is more easily attached to ITO than sulfonic acid and carboxylic acid. Furthermore, the results of UV-vis absorption spectra indicated that the –PO$_3$H-based SAMs have higher absorbance and coverage after self-assembly (Fig. 5(b)). Besides, sum-frequency generation vibrational spectroscopy of the –PO$_3$H-based SAMs displayed an ordered molecular orientation, which can enhance the interfacial dipole moment and adjust the interfacial band alignment in PSCs.[45] After washing the SAM-based conductive substrate, the –PO$_3$H-based substrate maintained the same absorbance, while that of the –COOH– and –SO$_3$H-based substrate exhibited a decline. The results demonstrated that the phosphonic acid-based TPT-P6 with the strongest anchoring strength achieved the best PCE of 21.43%, which is much higher than that of the –COOH– and –SO$_3$H-based SAMs. According to the comparison of anchoring groups, it is proven that the anchoring groups with a stronger bonding strength are beneficial for enhancing the assembly rate (coverage) and charge collection and suppressing interfacial recombination. In addition, the –PO$_3$H-based anchoring groups have better stability than the –COOH and –SO$_3$H groups.

5.1.4 The effect of the terminal group on the performance of SAMs. To investigate the effect of the terminal group (SAMs) on the performance of the device, different electron-donating and withdrawing functional groups (**23–27**, Fig. 6) were designed by Demic and co-authors.[46] The SAMs with terminal electron-withdrawing groups led to mismatched energy level alignment and formation of strong hydrogen bonding, which is
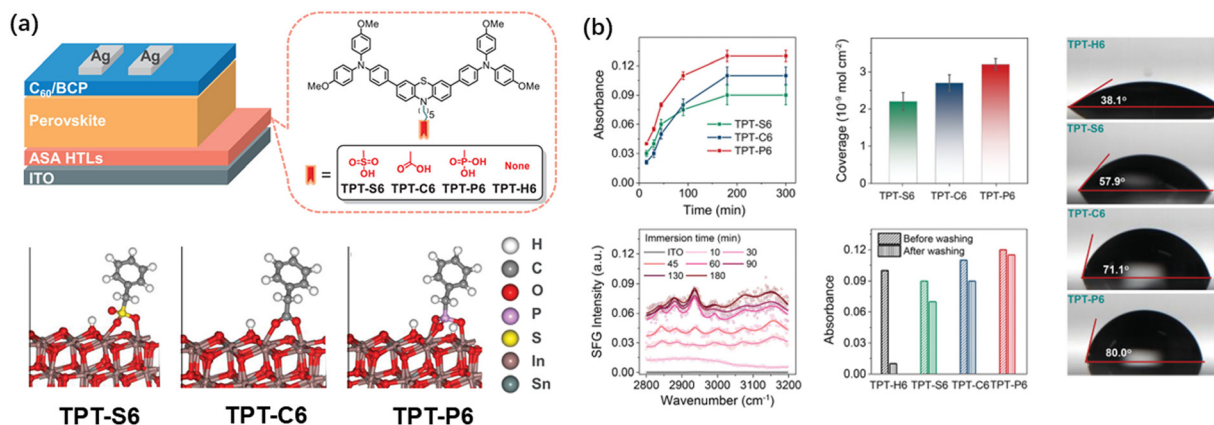
Fig. 5 (a) SAMs with various anchoring groups as HTLs for inverted PSCs. (b) Bonding strength-related absorbance and coverage of the SAMs with three anchoring groups. Reproduced with permission.[44] Copyright 2021, Wiley-VCH Verlag GmbH & Co. KGaA, Weinheim.
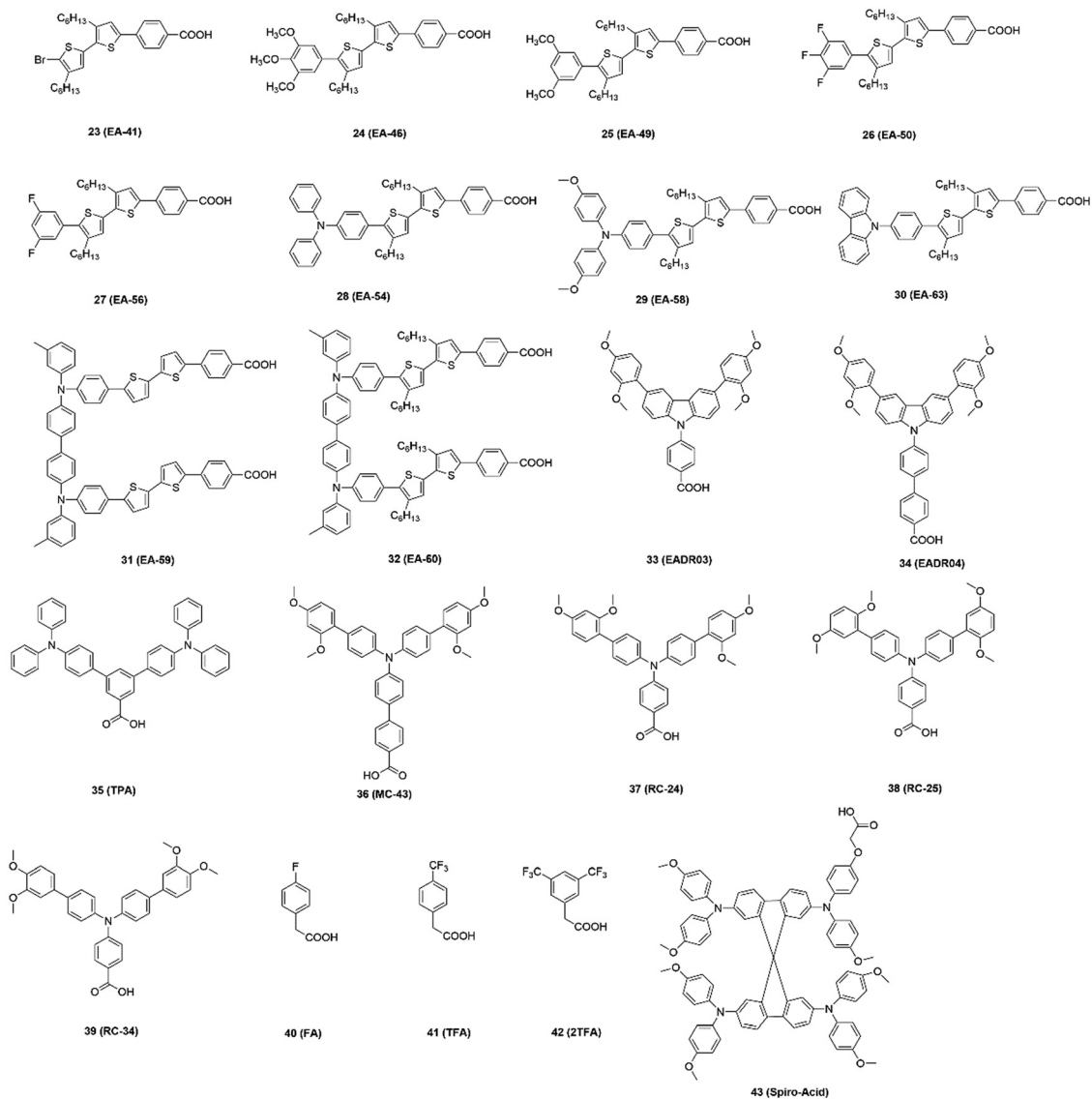
Fig. 6 Molecular structure of SAMs containing various terminal groups with carboxylic acid as the anchoring groups.

harmful for charge extraction, and thus the performance of PSCs. In addition, they also used various donor groups (**28–30**) to compare their photovoltaic performance.[47] The EA-58-based SAM has an appropriate energy level alignment and methoxy group that can passivate the trap states through coordinative bonding. The strategy of double anchoring groups was also applied in SAMs for PSCs. Demic and co-authors reported the preparation of two SAMs (EA-59:**31** and EA-60:**32**) with double anchoring groups to attach on the ITO substrate to tune the work function.[48]

Similarly, Palomares and co-authors[49] designed dimethoxy-benzene-substituted carbazole (**33** and **34**) as a donor for efficient charge selection and hole transfer, resulting in a smooth and compact perovskite film. This design enabled the perovskite devices to surpass 21% stabilized output efficiency. More importantly, the monolayer-based devices exhibited good stability compared to the PTAA-based cells. They also designed a

series of triphenylamine derivative-based SAMs (**35–39**) and tuned the substituted position on the donor part. It was found that the *para-* and *ortho*-substituted SAMs enabled the formation of a perovskite thin film with large grains grown atop, increasing the PCE to 20%.[50,51] Zhang *et al.*[52] introduced three SAMs with different numbers of F atoms (**40–42**) in phenyl-acetic acid to modify the surface work function (WF) of the ITO substrate with the formation of interfacial dipoles. Due to the optimized band structure and lower energy loss at the ITO/MAPbI$_3$ interface, the 2TFA-modified device achieved the highest power conversion efficiency (PCE) of 20.19%. There are also other examples exploring Spiro-OMeTAD derivative-based SAMs due to their good performances in regular devices. For instance, Palomares and co-authors[53] designed a Spiro-OMeTAD derivative with a carboxylic acid unit as the anchoring group to form SAMs (Spiro-Acid: **43**) for inverted PSCs, achieving a PCE of 18.15%.

5.1.5 Conjugated SAMs as HTLs in inverted PSCs. Although non-conjugated molecule-based SAMs have achieved some progress, conjugated molecule-based SAMs are also promising candidates for HTLs because of the fast charge transfer in conjugated structures. In addition, the conjugated part can improve the stability and delocalize the electrons in SAMs. The molecular structure of conjugated SAMs is shown in Fig. 7. According to the former experience in dye-sensitized solar cells (DSSCs), Guo and co-authors designed a D–π–A-structured molecule (MPA-BT-CA) as SAMs for HTLs in inverted PSCs.[54] The MPA-BT-CA-based SAMs could induce intramolecular charge transfer and contribute to fast hole extraction and reduce the charge recombination rate in PSCs, which achieved a PCE of 21.24%. Additionally, MPA-BT-CA also displayed a good performance in eco-friendly alcohol solvent with a PCE of 20.52%. The same group also attempted to optimize MPA-BT-CA and replace the anchoring groups with benzoic acid or rhodanine-3-propionic acid to form new SAMs (MPA-BT-BA and MPA-BT-RA, respectively).[55] They found that the SAMs with cyanoacrylic acid as the anchoring group had large dipole moments and formed a homogeneous layer on the ITO substrate. However, the SAMs with rhodanine-3-propionic acid as the anchoring groups tended to severely aggregate in the solid state due to the existence of sp^3-hybridized carbon atoms in the anchoring group. Moreover, the fluorine atom was introduced in the donor part to increase the dipole moment in the SAM (FMPA-BT-CA),[56] and consequently a remarkable PCE of 22.37% was achieved. As mentioned, the conjugation and intramolecular D–A characteristics can alter the carrier delocalization and molecular frontier energy levels. Accordingly, Zhu and co-authors[57] designed different donor units, including carbazole and triphenylamine, with varying electron-donating capabilities to gradually tune the energy level and match the valence band edge of the perovskite. In addition, they also changed the conjugation length to further manipulate

the self-assembly behavior of these SAMs. The optimal conjugated SAMs (MPA-Ph-CA) achieved a remarkably high PCE of 22.53%, which is even higher than that of the non-conjugated SAMs (MeO-2PACz, 21.29%). More importantly, the conjugated MPA-Ph-CA SAMs displayed better long-term stability than the non-conjugated MeO-2PACz under light excitation. These results for conjugated SAMs as HTLs in inverted PSCs show that the conjugated SAMs can help to achieve a good device performance and stability.

5.1.6 SAMs containing unpaired electron of N as anchoring group for the HTL in inverted PSCs. In the functional parts of SAMs, N (unpaired electrons) can also act as an anchoring group and interact with Sn in the ITO or FTO substrate (Fig. 8) because of the unpaired electron in the N atom. The N atom can be regarded as a Lewis base to interact with the conductive substrate, which is quite different from acid-based anchoring groups. Duan and co-authors[58] reported the synthesis of a series of triphenylamine derivatives (**55–57**) with the non-conjugated linker of sp^3-hybridized oxygen atom. The connection of the non-conjugated oxygen can simply adjust the suitable energy level at the ITO/SAM interface. In addition, the triphenylamine derivatives have small hole-reorganization energy due to the reduced variation in the torsion angle between the adjacent donor parts, which results in a matched energy level alignment, enhanced charge extraction and suppressed carrier recombination at the ITO/perovskite interface. As expected, the SAMs of DMeTPA-O delivered an increased performance of up to 20.57%.

A similar investigation was conducted by Curiel and co-authors,[59] who developed a convenient two-step procedure to synthesize a fused polyheteroaromatic (ADAI), which can spontaneously self-assemble to enhance the molecular arrangement to form ordered SAMs. Cheng and co-authors[60] reported that TAPC SAMs on ITO can induce the formation of an interfacial dipole at the ITO surface through the binding
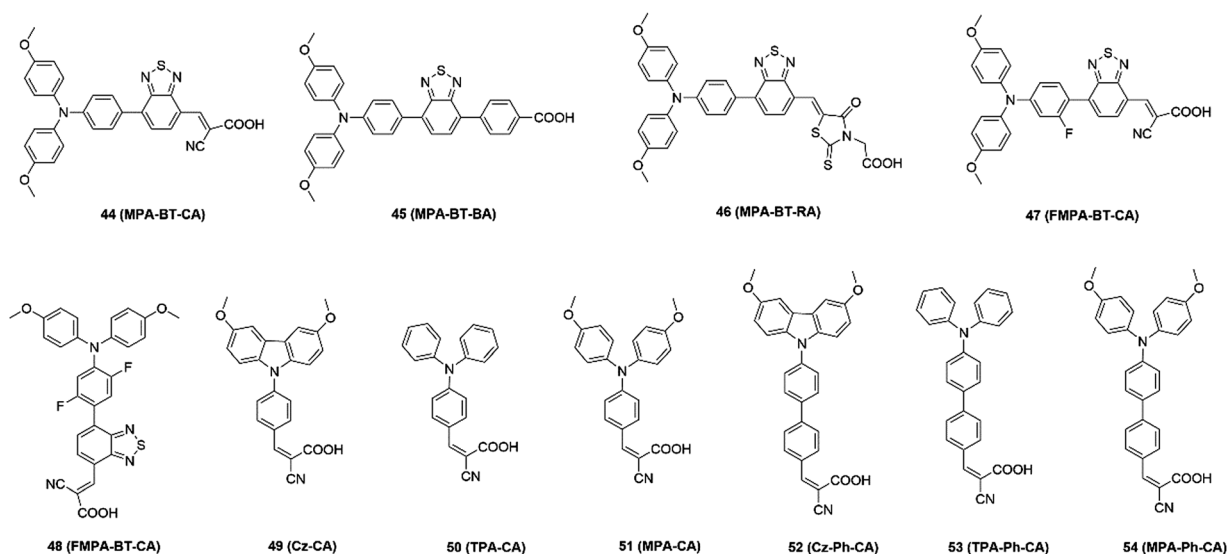
Fig. 7 SAMs containing a push–pull structure with conjugated unit in their linker.
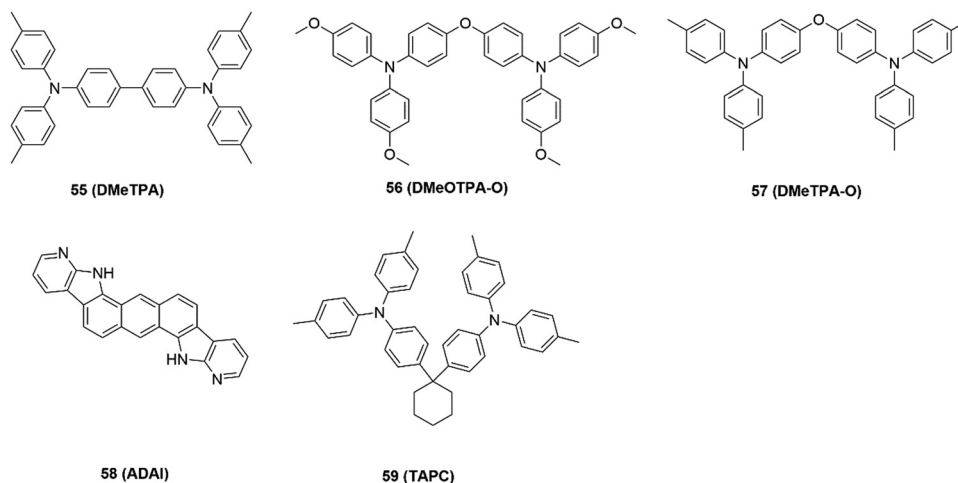
Fig. 8 SAMs with unpaired N as anchoring groups for HTL in inverted PSCs.

of Sn–N. It was found that the interfacial dipole of ITO/SAMs can increase the effective work function of ITO. By employing TAPC SAM-modified ITO as the substrate, the perovskite displayed upward energy band-bending at the interface of ITO/perovskite with decreased energy loss in the process of hole transfer from the perovskite to ITO. Consequently, the efficient hole transfer and extraction at the ITO/perovskite interface contributed to a PCE of over 19% for the TAPC-based device.

5.1.7 Polymer- and metal-based 2D materials as SAMs for HTL in inverted PSCs. Most SAMs are small organic molecules, while polymer and metal-based materials are rarely reported for PSCs (Fig. 9). Yan and co-authors[61] reported the preparation of a 2D conjugated metal–organic framework (Cu$_3$(HHTT)$_2$) and that the Cu ion could anchor on the conductive substrate

through interaction with –OH. Based on the crystal structure of the Cu-MOF-based SAMs, they observe the existence of strong π–π stacking between the adjacent layers. The Cu-MOF-based SAMs could provide an ultra-smooth surface for the growth of the perovskite and reduce the amount of defects on the buried perovskite surface. Consequently, a PCE of over 22% was obtained. In addition, a similar approach was found to be suitable for preparing large-area films and a PCE of 19.86% was achieved for the device with an area of 1 cm^2. Similarly, Wang and co-authors[62] designed self-assembling COOH-functionalized P3HT (P3HT–COOH) with an ultra-uniform morphology on the conductive substrate. Additionally, P3HT–COOH could form an ordered and homogeneous layer, which could facilitate the growth of a near single crystal perovskite thin film with high quality and preferred orientations. According
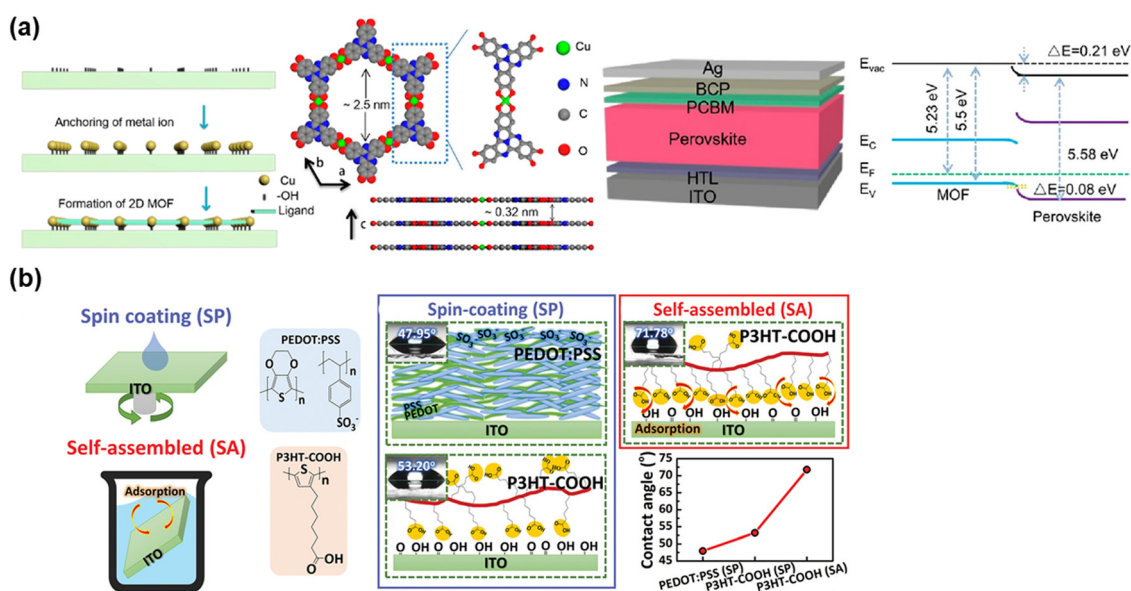
Fig. 9 SAMs as HTL for inverted PSCs. (a) Cu based-MOF 2D materials as ultrathin SAMs. Reproduced with permission.[61] Copyright 2022, the American Chemical Society. (b) Polymer-based SAMs. Reproduced with permission.[62] Copyright 2021, Wiley-VCH Verlag GmbH & Co. KGaA, Weinheim.

to the above-mentioned progress, the 2D metal MOF and polymer-based SAMs can form ordered and ultrasmooth molecules on the substrate, which is beneficial for the growth of perovskite films.

A summary of SAMs as HTLs in p–i–n-structured PSCs is listed in Table 1. It suggests that the SAMs (Me-4PACz) with carbazole as the terminal group and phosphonic acid as the anchoring group have the highest performance (PCE = 24.5%)

Table 1 A summary of SAMs as HTLs in p–i–n-structured PSCs

| SAMs	Perovskite	V_{oc} (V)	J_{sc} (mA cm^{-2})	FF (%)	PCE (%)	Ref.
V1036 + C4	$Cs_{0.05}(MA_{0.17}FA_{0.83})_{0.95}Pb(I_{0.83}Br_{0.17})_3$	1.09	21.4	76.5	17.8	29
V1036	$Cs_{0.05}(MA_{0.17}FA_{0.83})_{0.95}Pb(I_{0.83}Br_{0.17})_3$	1.041	21.2	79.3	17.5	30
MeO-2PACz	$Cs_{0.05}(MA_{0.17}FA_{0.83})_{0.95}Pb(I_{0.83}Br_{0.17})_3$	1.144	22.2	80.5	20.4	30
MeO-2PACz	$FA_{0.6}MA_{0.4}PbI_3$ (Sigle Crystal)	1.07	27.5	0.77	23.1	38
DC-PA + IAHA	$Cs_{0.05}MA_{0.15}FA_{0.80}PbI_3$	1.16	24.66	82.45	23.59	34
2PACz	$Cs_{0.05}(MA_{0.17}FA_{0.83})_{0.95}Pb(I_{0.83}Br_{0.17})_3$	1.188	21.9	80.2	20.9	30
4PACz	$Cs_{0.05}MA_{0.15}FA_{0.80}PbI_3$	1.07	23.20	58.43	14.5	35
Me-4PACz	$Cs_{0.05}MA_{0.22}FA_{0.73}Pb(I_{0.77}Br_{0.23})_3$	1.195	20.6	79.9	19.6	31
Me-4PACz + 6dPA	$FA_{0.79}MA_{0.16}Cs_{0.05}Pb(I_{0.83}Br_{0.17})_3$	1.168	21.1	79.2	19.2	36
CbzPh	$Cs_{0.05}MA_{0.15}FA_{0.80}PbI_3$	1.12	23.43	73.06	19.2	35
CbzNaph	$Cs_{0.05}MA_{0.15}FA_{0.80}PbI_3$	1.17	24.69	83.39	24.1	35
Me-4PACz	$Cs_{0.05}(FA_{0.92}MA_{0.08})_{0.95}Pb(I_{0.92}Br_{0.08})_3$	1.19	24.78	83.07	24.50	37
Br-2EPT	$Cs_{0.05}(FA_{0.92}MA_{0.08})_{0.95}Pb(I_{0.92}Br_{0.08})_3$	1.09	24.41	81.3	21.63	41
Br-2EPO	$Cs_{0.05}(FA_{0.92}MA_{0.08})_{0.95}Pb(I_{0.92}Br_{0.08})_3$	1.074	24.25	80.74	21.02	41
Br-2EPSe	$Cs_{0.05}(FA_{0.92}MA_{0.08})_{0.95}Pb(I_{0.92}Br_{0.08})_3$	1.12	24.49	82.86	22.73	41
MxPPA	$MAPbI_3$	0.68	16.84	0.51	5.92	42
MyPPA	$MAPbI_3$	0.79	16.67	0.57	7.57	42
PPA	$MAPbI_3$	0.94	16.18	0.57	8.81	42
CNPPA	$MAPbI3$	1.06	16.08	0.68	11.65	42
NPPA	$MAPbI_3$	1.07	18.44	0.70	13.94	42
PPA	$Cs_{0.05}FA_{0.85}MA_{0.1}PbI_3$	1.14	24.83	82.0	23.24	43
PPAOMe	$Cs_{0.05}FA_{0.85}MA_{0.1}PbI_3$	1.10	24.70	79.2	21.52	43
TPT-S6	$Cs_{0.05}MA_{0.12}FA_{0.83}Pb(I_{0.85}Br_{0.15})_3$	0.998	21.50	75.31	16.16	44
TPT-C6	$Cs_{0.05}MA_{0.12}FA_{0.83}Pb(I_{0.85}Br_{0.15})_3$	1.077	23.32	75.46	18.87	44
TPT-P6	$Cs_{0.05}MA_{0.12}FA_{0.83}Pb(I_{0.85}Br_{0.15})_3$	1.125	23.49	81.08	21.43	44
EA-41	$MAPbI_3$	1.019	16.69	69.86	11.89	46
EA-46	$MAPbI_3$	1.006	16.37	62.18	10.24	46
EA-49	$MAPbI_3$	1.024	17.25	68.15	12.03	46
EA-50	$MAPbI_3$	1.035	15.59	56.30	9.09	46
EA-56	$MAPbI_3$	1.023	15.05	56.56	8.71	46
EA-54	$MAPbI_3$	0.982	17.95	63.64	11.22	47
EA-58	$MAPbI_3$	0.967	18.56	76.37	13.71	47
EA-63	$MAPbI_3$	1.021	18.13	60.71	11.24	47
EA-59	$MAPbI_3$	1.043	17.68	71.56	13.19	48
EA-60	$MAPbI_3$	0.877	18.11	70.02	11.11	48
EADR03	$Cs_{0.05}FA_{0.79}MA_{0.16}Pb(I_{0.84}Br_{0.16})_3$	1.156	22.9	80	21.2	49
EADR04	$Cs_{0.05}FA_{0.79}MA_{0.16}Pb(I_{0.84}Br_{0.16})_3$	1.164	22.6	80	21.0	49
TPA	$MAPbI_3$	1.06	19.4	77	15.9	50
MC-43	$MAPbI_3$	1.07	20.3	80	17.3	50
RC-24	$Cs_{0.05}FA_{0.79}MA_{0.16}Pb(I_{0.84}Br_{0.16})_3$	1.123	22.3	79	19.8	51
RC-25	$Cs_{0.05}FA_{0.79}MA_{0.16}Pb(I_{0.84}Br_{0.16})_3$	1.116	22.1	79	19.6	51
RC-34	$Cs_{0.05}FA_{0.79}MA_{0.16}Pb(I_{0.84}Br_{0.16})_3$	1.109	22.5	79	19.7	51
FA	$MAPbI_3$	1.069	21.37	74.43	16.99	52
TFA	$MAPbI_3$	1.099	21.86	77.20	18.55	52
2TFA	$MAPbI_3$	1.120	22.24	81.06	20.19	52
Spiro-Acid	$Cs_{0.05}(FA_{0.85}MA_{0.15})_{0.95}Pb(I_{0.85}Br_{0.15})_3$	0.990	22.20	82.6	18.15	53
MPA-BT-CA	$(FA_{0.17}MA_{0.94}PbI_{3.11})_{0.95}(PbCl_2)_{0.05}$	1.13	22.25	84.8	21.24	54
MPA-BT-BA	$(FA_{0.17}MA_{0.94}PbI_{3.11})_{0.95}(PbCl_2)_{0.05}$	1.12	22.76	81.0	20.58	54
MPA-BT-RA	$(FA_{0.17}MA_{0.94}PbI_{3.11})_{0.95}(PbCl_2)_{0.05}$	1.10	22.03	81.1	19.65	55
FMPA-BT-CA	$(FA_{0.17}MA_{0.94}PbI_{3.11})_{0.95}(PbCl_2)_{0.05}$	1.151	23.33	83.3	22.37	56
2FMPA-BT-CA	$(FA_{0.17}MA_{0.94}PbI_{3.11})_{0.95}(PbCl_2)_{0.05}$	1.143	22.81	83.1	21.68	56
Cz-CA	$(Cs_{0.05}(FA_{0.92}MA_{0.08})_{0.95}Pb(I_{0.92}Br_{0.08}))_3$	1.07	23.2	81.3	20.17	57
TPA-CA	$(Cs_{0.05}(FA_{0.92}MA_{0.08})_{0.95}Pb(I_{0.92}Br_{0.08}))_3$	1.04	22.8	74.2	17.58	57
MPA-CA	$(Cs_{0.05}(FA_{0.92}MA_{0.08})_{0.95}Pb(I_{0.92}Br_{0.08}))_3$	1.08	23.4	80.6	20.36	57
Cz-Ph-CA	$(Cs_{0.05}(FA_{0.92}MA_{0.08})_{0.95}Pb(I_{0.92}Br_{0.08}))_3$	1.11	23.0	80.9	20.66	57
TPA-Ph-CA	$(Cs_{0.05}(FA_{0.92}MA_{0.08})_{0.95}Pb(I_{0.92}Br_{0.08}))_3$	1.12	23.1	78.3	20.26	57
MPA-Ph-CA	$(Cs_{0.05}(FA_{0.92}MA_{0.08})_{0.95}Pb(I_{0.92}Br_{0.08}))_3$	1.139	23.55	84.02	22.53	57
DMeOTPA-O	$Cs_{0.05}(FA_{0.88}MA_{0.12})_{0.95}PbI_3$	0.97	23.82	80.8	18.67	58
DMeTPA-O	$Cs_{0.05}(FA_{0.88}MA_{0.12})_{0.95}PbI_3$	1.01	24.93	81.7	20.57	58
DMeTPA	$Cs_{0.05}(FA_{0.88}MA_{0.12})_{0.95}PbI_3$	1.00	24.31	80.5	19.57	58
ADAI	$MAPbI_3$	1.04	19.9	77	15.5	59
TAPC	$MAPbI_{3-x}Cl_x$	1.12	22.07	78.89	19.42	60
P3HT-COOH	$MAPbI_3$	1.10	22.83	82.6	20.74	62

in organic–inorganic hybrid perovskites *via* the method of co-deposition.[37] In addition, it can also be found that the SAMs with phosphonic acid as the anchoring group can achieve better performance among the various anchoring groups. For the linker, it should be noted that a too long length in the linker will create large interfacial resistance. More importantly, the strategy of using binary SAMs can provide an effective way to solve the issue of wettability. SAMs as HTLs have also displayed desirable performances in Sn-based PSCs, as summarized in Table 2. The devices (Sn absorber) with SAMs as HTLs have better thermal stability than PEDOT:PSS-based devices. However, the application of SAMs in lead-free and all-inorganic perovskite is still rare. Thus, the development of more SAMs with high-stability suitable energy levels is necessary.

5.2 SAMs as interfacial modification layers for NiO_x-or PEDOT:PSS-based PSCs

NiO_x and PEDOT:PSS are commonly used HTLs in inverted PSCs.[63–66] However, there are still many issues to be solved such as low hole mobility and instability. Jen and co-authors[67] used a series of benzoic acid SAMs (Fig. 10(a)) with different dipole moments to passivate the surface defects in NiO_x nanoparticles (NPs) and found that 4-bromobenzoic acid could effectively play a

role in surface passivation. In addition, the V_{oc} of the device is related to the direction and strength of the dipole moments of the SAMs. The SAM layer reduced the trap-assisted recombination, minimized the energy offset between the NiO_x NPs and perovskite, and changed the wettability of the HTL surface, thus enhancing the crystallization of the perovskite and resulting in more stable PSCs with an enhanced PCE to 18.4%. Wang and co-authors[68] designed and synthesized two pyridine-terminated conjugated small organic molecules (Fig. 10(b)) to link the NiO_x and perovskite layers for NiO_x-based perovskite solar cells (PSCs). Surface modification of the NiO_x film with the PTZ molecules contributed to the efficient hole extraction, reduced defect density and prohibited interfacial charge recombination. Min and co-authors[69] used the bidentate chelating ligand 2,2′-bipyridine (Fig. 10(c)) to modulate the interfacial properties between NiO_x and perovskite *via* its strong interactions between the two layers. The improved interfacial contact is beneficial to the crystal growth of the perovskite. Similarly, Yang and co-authors[70] reported the use of an ethanolamine molecule monolayer (Fig. 10(d)) to modify the NiO_x nanocrystal layers, which could enhance the hole extraction/transport, and thus the photovoltaic performance.

Chen and co-authors[71] reported the use of *p*-chlorobenzene-sulfonic acid (CBSA, Fig. 11(a)) SAMs to simultaneously anchor

Table 2 A summary of SAMs as HTLs in p−i−n-structured PSCs with Sn as the absorber

SAMs	Perovskite	V_{oc} (V)	J_{sc} (mA cm^{-2})	FF (%)	PCE (%)	Ref.
MeO-2PACz	$FASnI_3$	0.458	19.5	67.4	6.02	32
2PACz	$FASnI_3$	0.320	11.7	47.0	1.8	32
2PACz	$Cs_{0.025}FA_{0.475}MA_{0.5}Sn_{0.5}Pb_{0.5}I_{2.925}Br_{0.075}$	0.86	32.83	0.76	21.39	33
MPA	$Cs_{0.025}FA_{0.475}MA_{0.5}Sn_{0.5}Pb_{0.5}I_{2.925}Br_{0.075}$	0.84	32.75	0.77	21.08	33
2PACz + MPA	$Cs_{0.025}FA_{0.475}MA_{0.5}Sn_{0.5}Pb_{0.5}I_{2.925}Br_{0.075}$	0.88	33.13	0.80	23.23	33
$Cu_3(HHTT)_2$	$FA_{0.83}Cs_{0.17}Sn_{0.35}Pb_{0.65}I_{2.9}Br_{0.1}$	0.92	30.13	79.42	22.01	61
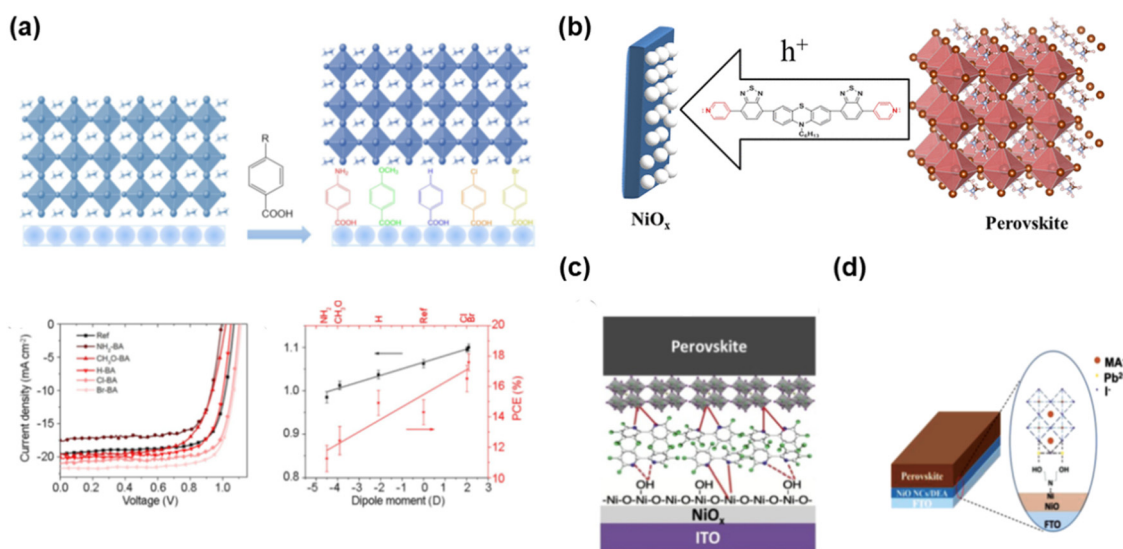
Fig. 10 SAMs as interfacial modification layers for NiO_x-based PSCs. (a) Benzoic acid derivatives with various dipole moments. Reproduced with permission.[67] Copyright 2017, Wiley-VCH Verlag GmbH & Co. KGaA, Weinheim. (b) Push–pull-structured pyridine SAMs in NiO_x-based device. Reproduced with permission.[68] Copyright 2019, the American Chemical Society. (c) Bipyridine-based SAMs deposited on NiO_x. Reproduced with permission.[69] Copyright 2019, Elsevier B.V. (d) Ethanolamine SAMs in NiO_x-based devices. Reproduced with permission.[70] Copyright 2016, Wiley-VCH Verlag GmbH & Co. KGaA, Weinheim.

This journal is © The Royal Society of Chemistry and the Chinese Chemical Society 2023

NiO_x and perovskite crystals, which could realize bifunctional passivation. Due to the existence of chlorine, the SAMs afforded growth sites for the perovskite and contributed to the interfacial strain release and filled the iodine vacancies. In addition, the anchoring group ($-SO_3H$) in the SAMs can passivate the surface defects of NiO_x. More importantly, the formed SAMs can restrict the unfavorable redox reaction at the NiO/perovskite interface, which is beneficial for improving the charge carrier extraction and stability. Therefore, the NiO_x/CBSA-based PVSCs obtained a champion PCE of 21.8% with enhanced thermal stability, which could maintain over 80% of its initial PCE after tracking at 80 °C for 800 h under an N_2 atmosphere. The carbazole phosphonic acid (2PACz, Fig. 11(b)) SAMs could also be used to modify an NiO_x film with a PCE of 22.2%.[72] In addition, 2PACz SAMs on the substrate of PEDOT-PSS offered an energetically aligned interface at the HTL/Sn-based perovskite absorber interface (Fig. 11(c)), which contributed to less lattice disordering and reduced charge recombination in the perovskite film.[73] Due to the absence of direct contact between PEDOT:PSS and the perovskite film, a perovskite film with a compact morphology was formed on the substrate and further improve the stability of the device with a PCE of 8.66% for the tin based-device. The same strategy was used by Na and co-authors,[74] who reported the preparation of 3-(triethoxysilyl)-propylamine (TSPA, Fig. 11(d)) SAMs on NiO_x through hydrogen-bonds between the amino group of TSPA and hydroxyl group on the surface of NiO_x, which can reduce the surface defects and avoid the direct contact of the hydroxyl groups and the perovskite to improve the stability. Furthermore, by inserting TSPA SAMs in NiO_x, a positive dipole moment was formed and pointed toward the surface of NiO_x, which contributed to

the suitable work function at the NiO_x interface with matched energy level alignment with the VB of the perovskite grown atop. Finally, after treatment with TSPA, the interface showed improved charge extraction/transportation capability and reduced charge recombination. Zhu and co-authors[75] reported an interfacial dipole with $-CF_3$-terminated silane SAMs (Fig. 11(e)) connected to the NiO_x/perovskite interface, leading to well matched energy levels and notably reduced energy barrier. Additionally, the insertion of Si–CF_3 improved the conductivity of NiO_x and the formed dipole interlayer could adjust the built-in electric field, which finally improved the current density and photovoltage simultaneously. Eventually, the modified device achieved a PCE of 19.58%, which is much better than that of 17.98% of the control device.

A summary of SAMs as interfacial layers for NiO-based PSCs is presented in Table 3. Firstly, to improve the voltage of the NiO-based device, the SAMs should have their dipole moment pointed toward the NiO substrate. Secondly, the conjugated linker of SAMs can increase the charge transfer rate between the perovskite and NiO. Moreover, the interaction between the terminal group of SAMs with Pb^{2+} is important for the preparation of high-quality perovskite films.

6. SAMs as electron transporting layers or modifying layers for n–i–p-structured PSCs

6.1 SAMs as electron transporting layers for n–i–p-structured PSCs

Besides application as the hole transport layers, SAMs can also be used as electron transport layers for n–i–p-based PSCs (Fig. 12),
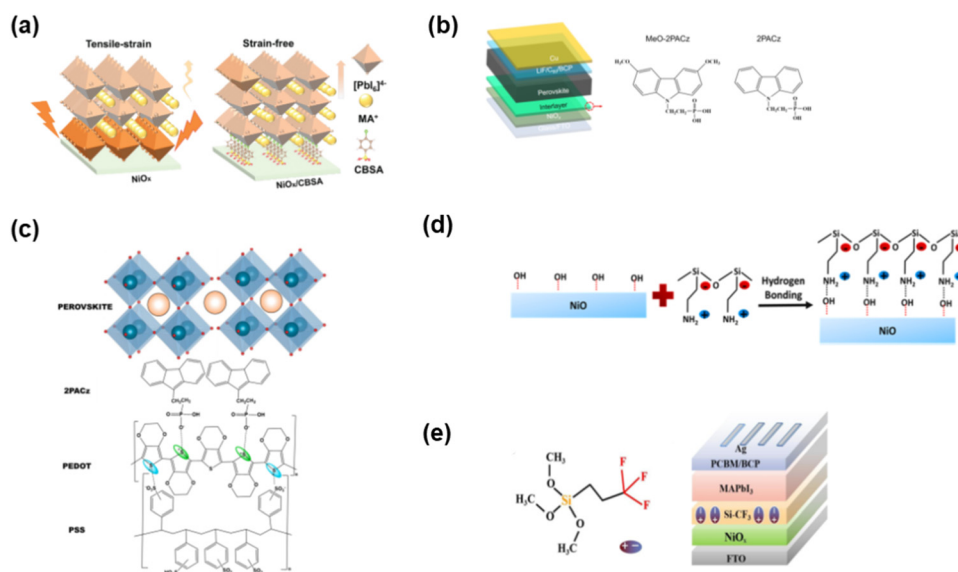
Fig. 11 (a) p-Chlorobenzenesulfonic acid SAMs in NiO_x-based device. Reproduced with permission.[71] Copyright 2022, Wiley-VCH Verlag GmbH & Co. KGaA, Weinheim. (b) Carbazole derivative SAMs in NiO_x-based device. Reproduced with permission.[72] Copyright 2022, Elsevier B.V. (c) Carbazole derivative SAMs in PEDOT:PSS-based devices. Reproduced with permission.[73] Copyright 2022, Elsevier B.V. (d) Silane SAMs in NiO_x-based device. Reproduced with permission.[74] Copyright 2022, Elsevier B.V. (e) –CF_3 group-substituted silane SAMs. Reproduced with permission.[75] Copyright 2021, Elsevier B.V.

Table 3   SAMs as interfacial layers for NiO- or PEDOT:PSS-based PSCs

SAMs	Perovskite	V_{oc} (V)	J_{sc} (mA cm^{-2})	FF (%)	PCE (%)	Ref.
NiO/Br-BA	MAPbI$_3$	1.11	21.7	76.3	18.4	67
NiO/NH$_2$-BA	MAPbI$_3$	0.99	17.5	74.1	12.8	67
NiO/CH$_3$O-BA	MAPbI$_3$	1.02	19.1	70.6	13.8	67
NiO/H-BA	MAPbI$_3$	1.05	20.3	76.2	16.2	67
NiO/Cl-BA	MAPbI$_3$	1.10	21.0	76.0	17.6	67
NiO/PTZ-1	MAPbI$_3$	1.028	20.91	75.6	16.25	68
NiO/PTZ-2	MAPbI$_3$	1.043	21.45	76.0	17.00	68
NiO/BiPy	CsFAMA	1.08	19.81	77.26	16.53	69
NiO/DEA	MAPbI$_{3-x}$Cl$_x$	0.95	20.90	80	15.90	70
NiO/CBSA	Cs$_{0.05}$(FA$_{0.92}$MA$_{0.08}$)$_{0.95}$(I$_{0.92}$Br$_{0.08}$)$_3$	1.11	24.01	81.43	21.8	71
NiO/2PACz	FA$_{0.79}$MA$_{0.16}$Cs$_{0.05}$Pb(I$_{0.9}$Br$_{0.1}$)$_3$	1.13	23.6	82.5	22.4	72
NiO/MeO-2PACz	FA$_{0.79}$MA$_{0.16}$Cs$_{0.05}$Pb(I$_{0.9}$Br$_{0.1}$)$_3$	1.09	23.4	82.5	21.0	72
PEDOT:PSS/2PACZ	**Sn perovskite**[a]	0.74	16.22	73	8.66	73
NiO/Si-CF$_3$	MAPbI$_3$	1.10	22.45	79.3	19.58	74
NiO/TSPA	CsFAMA	1.11	22.76	80.32	20.21	75

[a] Sn perovskite: EDA$_{0.01}$(GA$_{0.06}$(FA$_{0.8}$Cs$_{0.2}$)$_{0.94}$)$_{0.98}$SnI$_2$Br.
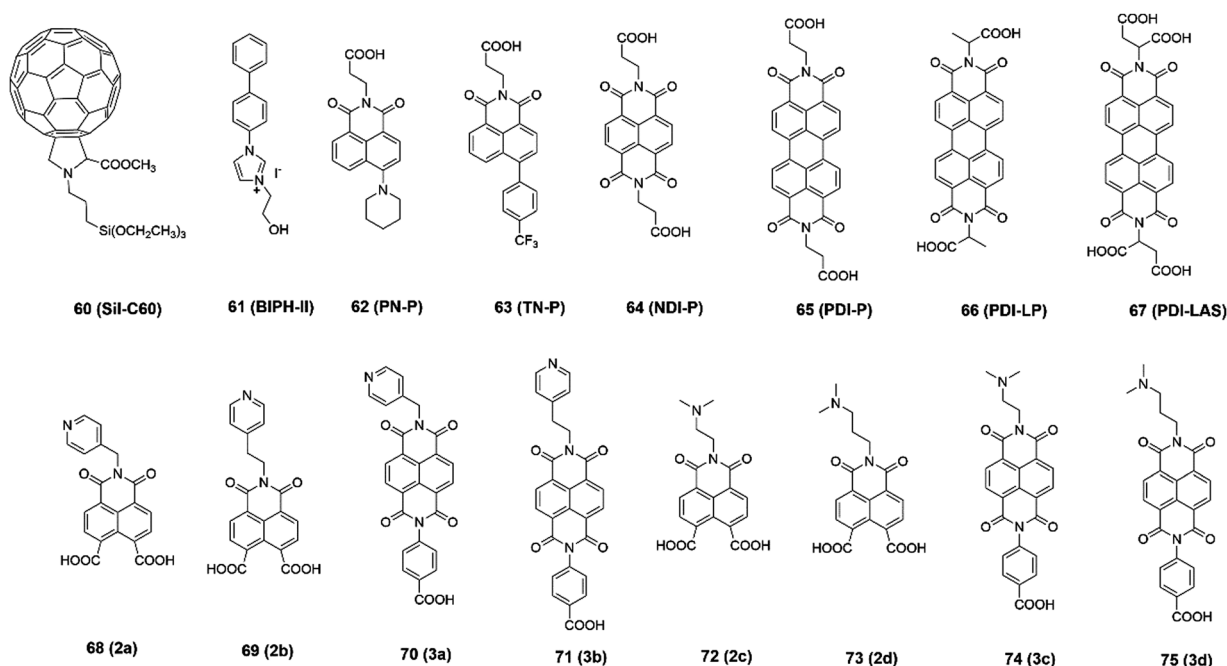

Fig. 12   Molecular structure of SAMs as electron transport layers for n−i−p-structured PSCs.

which can also play a role in the passivation of defects and adjusting the energy level. Due to the good conductivity of fullerene, Petrozza and co-authors designed a self-assembled siloxane-functionalized fullerene molecule as the ETL for n–i–p-based PSCs with a PCE of 15%.[76] Besides fullerenes, n-type molecules such as imidazolium iodide-functionalized ionic liquid also displayed ability to tune the work function of the FTO substrate, and then increase the PCE to 17.31%.[77]

Due to their good thermal stabilities and high electron mobility, naphthalene-imide derivatives are very promising candidates as electron transporting materials. Zhu and co-authors[78,79] reported a series of naphthalimide derivatives substituted with electron-rich piperidine (PN-P), 4-trifluoromethylphenyl (TN-P), and electron-deficient imide (NDI-P)

groups. Because of the improved interfacial energetic alignment, NDI-P exhibited the most efficient electron extraction capability with a PCE of 16%. Compared with NDI, PDI derivatives have more suitable LUMO energy levels aligned with the CB edge of perovskites, which reduces the electron transfer barrier and facilitates the interfacial electron extraction. In addition, the incorporation of branched anchoring chains can efficiently address the solubility issue of PDI compounds and increase their solution processability. Consequently, the PDI-LAS-based SAM achieved a PCE of 18.77%. Bach and co-authors[80] designed eight naphthalene imide derivatives as SAMs on ITO as ETLs for PSCs. The pyridines and amines in the terminal group of the SAMs can coordinate with Pb^{2+} ions, and then stabilize the perovskite surface. Their results indicated that the more Lewis

Table 4 The SAMs as ETLs in n–i–p-based PSCs

SAMs	Perovskite	V_{oc} (V)	J_{sc} (mA cm^{-2})	FF (%)	PCE (%)	Ref.
Sil-C60	$Cs_{0.05}FA_{0.75}MA_{0.2}PbBr_{0.3}I_{2.7}$	1.04	19.4	74	15.2	76
BIPH-II	$MAPbI_3$	1.082	22.40	71.4	17.31	77
PN-P	$MAPbI_3$	0.76	10.23	69.68	5.45	78
TN-P	$MAPbI_3$	0.94	10.93	52.94	5.41	78
NDI-P	$MAPbI_3$	1.05	20.56	73.98	16	78
PDI-LP	$MAPbI_3$	1.08	22.57	72.81	17.83	79
PDI-LAS	$MAPbI_3$	1.11	22.88	73.98	18.77	79
2a	$Cs_{0.05}FA_{0.8}MA_{0.15}PbI_{2.5}Br_{0.5}$	1.03	20.0	0.62	12.6	80
2b	$Cs_{0.05}FA_{0.8}MA_{0.15}PbI_{2.5}Br_{0.5}$	1.01	19.7	0.62	12.4	80
2c	$Cs_{0.05}FA_{0.8}MA_{0.15}PbI_{2.5}Br_{0.5}$	0.95	20.4	0.57	11.1	80
2d	$Cs_{0.05}FA_{0.8}MA_{0.15}PbI_{2.5}Br_{0.5}$	1.01	19.8	0.60	12.1	80
3a	$Cs_{0.05}FA_{0.8}MA_{0.15}PbI_{2.5}Br_{0.5}$	0.95	20.5	0.54	10.5	80
3b	$Cs_{0.05}FA_{0.8}MA_{0.15}PbI_{2.5}Br_{0.5}$	1.01	19.6	0.62	12.2	80
3c	$Cs_{0.05}FA_{0.8}MA_{0.15}PbI_{2.5}Br_{0.5}$	0.99	19.8	0.56	10.9	80

base SAMs acted as a better passivation agent for the perovskite, which could reduce the surface recombination velocities and increase the efficiency. In addition, the two carboxylic acid anchoring group-based SAMs exhibited better coverage on ITO than the benzoic acid-based SAMs, which provided better electronic coupling between ITO and the perovskite. Eventually, the naphthalene-imide SAM (3a) could maintain 80% of the original PCE at the temperature of 85 °C for 800 h. The above-mentioned reports are summarized in Table 4, where it can clearly be seen that the fullerene and naphthalene imide derivative-based SAMs are good candidates as the ETL for n–i–p-based PSCs because of their high electron mobility and thermal stability.

6.2 SAMs as interfacial modification layers for TiO₂-based PSCs

As a n-type semiconductor, TiO₂ has been widely used in PSCs as the electron transport layers.[81–83] However, the presence of oxygen-based unoccupied sites and their poor UV stability affect the performance of the device. In the case of planar PSCs, Snaith and coworkers[84] used fullerene-based SAMs (C₆₀-SAM) to modify the compact TiO₂ surface (Fig. 13(a)) and investigated the physical processes occurring at the interface between the ETL and perovskite by photothermal deflection spectroscopy and photoluminescence analysis. Their results showed that the C₆₀-SAM enhanced the electron transfer rate and reduced the hysteresis behavior. For the mesoporous TiO₂-based device (Fig. 13(b)), the C₆₀-SAM acted as an electron acceptor but inhibited further electron transfer to the mesostructured TiO₂ due to their energy level misalignment and poor electronic coupling. The PCE of the C₆₀-SAM and P3HT-based device was only 6.7%, but further increased to 11.7% after applying Spiro-OMeTAD as the HTL.[85] Hayase and co-authors[86] applied HOOC-R-NH₃I-based SAMs (Fig. 13(c)) at the interface between perovskite and mesoporous TiO₂. The SAMs could retard the charge recombination and enhance the growth of the perovskite crystal. Consequently, the PCE increased from 8% to 12%. Han and co-authors[87] reported the preparation of an organic silane-based SAM (Fig. 13(d)) on mesoporous TiO₂ for hole-conductor-free PSCs with a carbon counter electrode,

leading to optimized interfacial band alignment and enhanced charge lifetime. The PCE improved from 9.6% to 12.7%. Thus, these results indicate that C60, amino-acid and organic silane-based SAMs have a good passivation effect on the interface of TiO₂/perovskite and improve the charge lifetime by reducing the defects.

Besides the above-mentioned SAMs used for TiO₂, Meng and co-authors[88] reported the strategy of synergistic SAM (Fig. 14(a)), which can passivate the defects and enhance the charge transfer simultaneously. They utilized 3-carboxypropyl-triphenyl phosphonium bromide (CPTPB) together with a fullerene derivative (PCBA) to self-assemble at the TiO₂/perovskite interface. They showed that the interaction of hydrogen bonding among CPTPB, PCBA, and TiO₂ can contribute to the formation of functionalized C-PCBA SAMs. More importantly, the appropriate conjugated structure in CPTPB could facilitate the orderly bonding of the SAMs to the TiO₂ substrate. Consequently, a maximum PCE of 24.8% could be realized for the planar TiO₂-based PSCs with a high operational stability, which could maintain 85% of their initial PCE after 700 h continuous light illumination. Pauporté and co-authors[89] reported the attachment of chloride-functionalized benzoic acid molecules (CBA) at the TiO₂ surface through a bridging bidentate mode. In addition, the Cl in the CBA SAMs has strong binding with the perovskite. Through the experimental analysis and theoretical calculation, it can be concluded that the CBA SAMs at the oxide/perovskite interface contributed to the continuous structure, reduced defects, and high quality of the perovskite film atop (Fig. 14(b)). The PCE of the CBA SAM-modified device increased from 20.3% to 21.35%. Jia and co-authors[90] reported the use of bifunctional SAMs (4-picolinic acid, Fig. 14(c)) as an interface linker to facilitate the charge transfer and passivate the defects at the interface of TiO₂/perovskite. Zheng and co-authors[91] introduced SAMs with double anchoring groups, i.e., carboxylic acid and thiol groups (HOOC–Ph–SH, Fig. 14(d)), to link the interface between the porous TiO₂ and perovskite layers and enhance the electron transfer. In addition, modifying the top surface of perovskite with hydrophobic thiols (HS-PhF5) could effectively improve the stability of the PSCs because of the strong binding between S and Pb. Tao and co-authors[92]
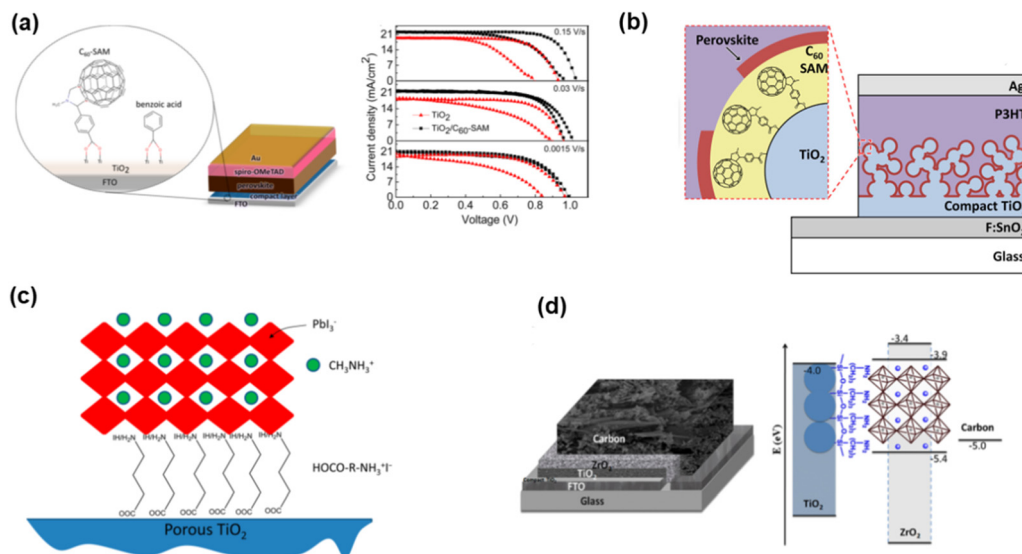
Fig. 13 SAMs in TiO$_2$-based perovskite solar cells. (a) C$_{60}$-SAM deposited on planar TiO$_2$-based device. Reproduced with permission.[84] Copyright 2014, the American Chemical Society. (b) C$_{60}$-SAM attached on mesoporous TiO$_2$-based devices. Reproduced with permission.[85] Copyright 2013, American Chemical Society. (c) HOOC−(CH$_2$)$_3$−NH$_3$I on mesoporous TiO$_2$-based device. Reproduced with permission.[86] Copyright 2014, the American Chemical Society. (d) Organic silane self-assembled monolayer on mesoporous TiO$_2$-based device. Reproduced with permission.[87] Copyright 2015, the American Chemical Society.
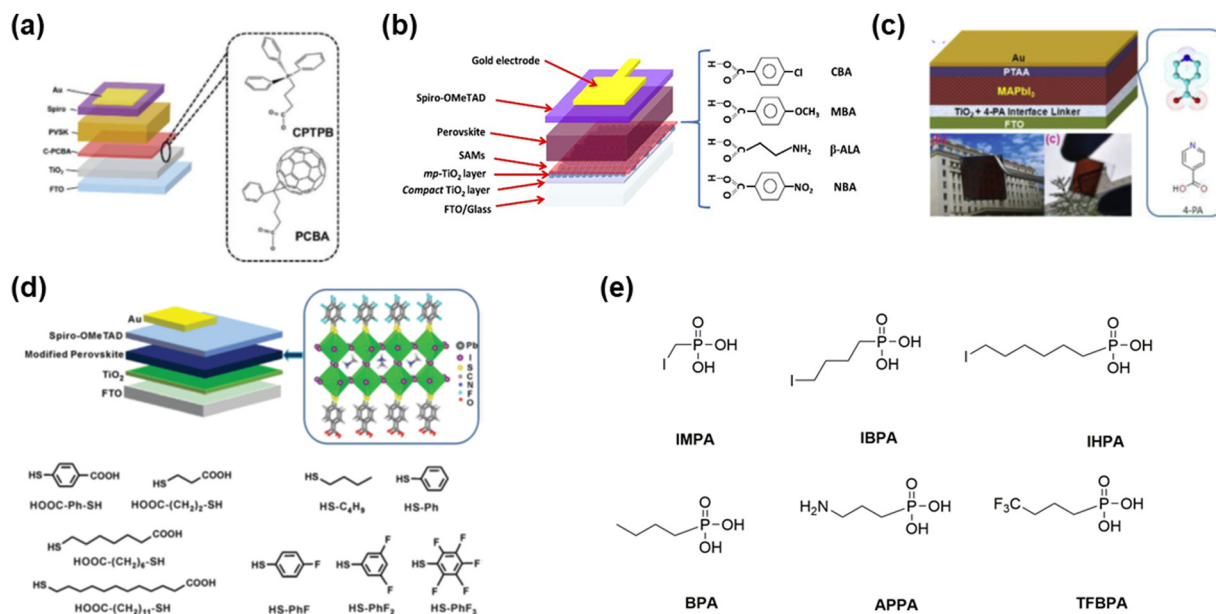
Fig. 14 SAMs in TiO$_2$-based perovskite solar cells: (a) 3-carboxypropyl-triphenyl phosphonium bromide with the fullerene derivative in planar TiO$_2$-based device. Reproduced with permission.[88] Copyright 2022, Wiley-VCH Verlag GmbH & Co. KGaA, Weinheim. (b) Benzoic acid and amino acid derivative-based SAMs in mesoporous TiO$_2$-based devices. Reproduced with permission.[89] Copyright 2020, the American Chemical Society. (c) 4-Picolinic acid in mesoporous TiO$_2$-based device. Reproduced with permission.[90] Copyright 2019, Elsevier B.V. (d) Thiol-based SAMs in mesoporous TiO$_2$-based device. Reproduced with permission.[91] Copyright 2015, The Royal Society of Chemistry. (e) Phosphonic acid-based SAMs in mesoporous TiO$_2$-based device.

designed a series of phosphonic acid-based SAMs (Fig. 14(e)) with different chain lengths and terminal functional groups to modify the mesoporous TiO$_2$ surface and investigate their effect on charge extraction. It was found that the longer chain length of the linker led to large tunnelling barrier and decreased

performance. Although the terminal group adjusted the energy level at the TiO$_2$/perovskite interface, the chemical interaction between the terminal group and perovskite is more important to achieve high performance due to its influence on the morphology of the perovskite film and charge extraction.

6.3 SAMs as interfacial modification layers for SnO_2-based PSCs

The high performance of TiO_2-based ETLs usually requires high temperature processes to form a mesoporous structure. You and co-authors[93] used SnO_2-based nanoparticles to prepare efficient SnO_2-based planar PSCs. Since then, increasing work has been focused on SnO_2-based ETLs.[94] Padture and co-authors[95] reported the use of I-SAM (3-iodopropyl trimethoxysilane, Fig. 15(a)) to modify SnO_2, which could apparently increase the interfacial adhesion between SnO_2 and the perovskite film, and then enhance the mechanical reliability. After treatment with I-SAM on SnO_2, the PCE increased from 20.2% to 21.4% with low hysteresis and improved operational stability. Moreover, after continuous maximum power point tracking for 4000 h under 1 sun illumination, the I-SAM-based device could maintain 80% of its initial PCE. In contrast, the control device showed extensive irreversible morphological degradation at the SnO_2/perovskite interface, including the formation of voids and delamination. The enhanced stability in the I-SAM-treated device was attributed to the decreased concentration of hydroxyl groups at the interface and the higher interfacial adhesion.

Besides the factor of passivating the defects in the SnO_2-based ETL, the mechanism of SAMs in improving the performance of SnO_2/perovskite-based devices can also originate from other factors. For example, the coordination SAM and Pb^{2+} and the improved quality of the film. Hayase and co-authors[96] developed a facile route for interfacial sulfur functionalization by employing xanthate decomposition (Fig. 15(b)) on SnO_2. The sulfur atoms at the interface can coordinate with Pb^{2+} in the perovskite film and passivate its surface, which is favorable for the growth of perovskite crystals, leading to better surface morphology and enhanced crystallinity with a larger perovskite grain size. Yang and co-authors[97] reported the use of van der Waals and dipolar interaction based-SAMs (Fig. 15(c)) to modify SnO_2. The device performance of the PSCs with various SAMs was opposite with their corresponding energy level alignment. The results proved that the interfacial chemical interactions are the main factor in affecting the performance of PSCs in this system. Consequently, the PA-SAM achieved the highest PCE of 18.8% due to the strong chemical interaction between the terminal pyridine with perovskite, which could reduce the defects and contribute to the interfacial charge transfer. According to the results in the above-mentioned reports, the chemical interactions between SAMs and perovskite should be considered in the molecular design of SAMs for highly efficient PSCs.

Together with the above-mentioned SAMs, salt-based SAMs have also been reported. Chen and co-authors[98] reported a novel type of sulfonium salt (2-carboxyethyl) dimethyl sulfonium chloride-based SAMs (CDSC, Fig. 16(a)) to modify the interface between perovskite and SnO_2. Through theory and experiment, it was revealed that CDSC can chemically interact with both SnO_2 and the perovskite layer, which can be regarded as a bridge to link both layers and reduce the interfacial energy barrier by improving the energetic alignment. The PCE of the SnO_2/CDSC-based device improved to 22.44%. Besides the above-mentioned sulfonium salt-based SAM, the use of ammonia acid (HOOC–R–NH_2) as SAMs for the ETL/perovskite interface has also been reported in TiO_2-based devices. Chang and co-authors[99] introduced an amino acid self-assembled layer
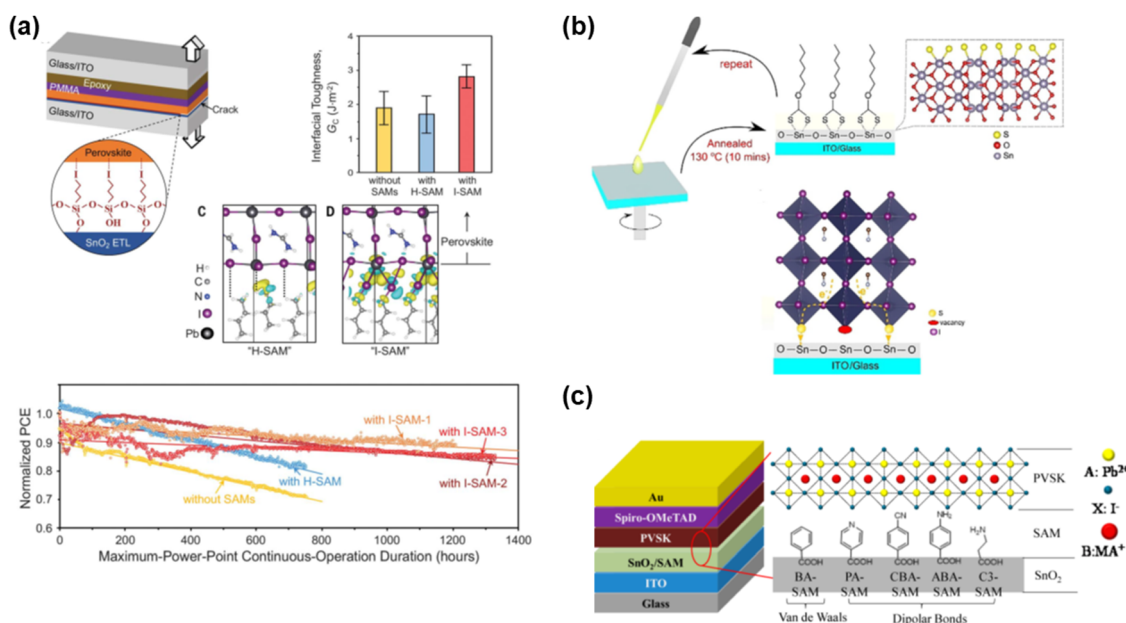
Fig. 15 SAMs as interfacial modification layers for SnO_2-based PSCs (a) organic silane-based SAMs with various terminal groups in SnO_2-based device. Reproduced with permission.[95] Copyright 2021, Science Press. (b) Thiol-based SAMs in SnO_2-based device. Reproduced with permission.[96] Copyright 2018, Wiley-VCH Verlag GmbH & Co. KGaA, Weinheim. (c) Benzoic acid derivative-based SAMs with van der Waals or dipolar bonds in SnO_2-based devices. Reproduced with permission.[97] Copyright 2017, the American Chemical Society.
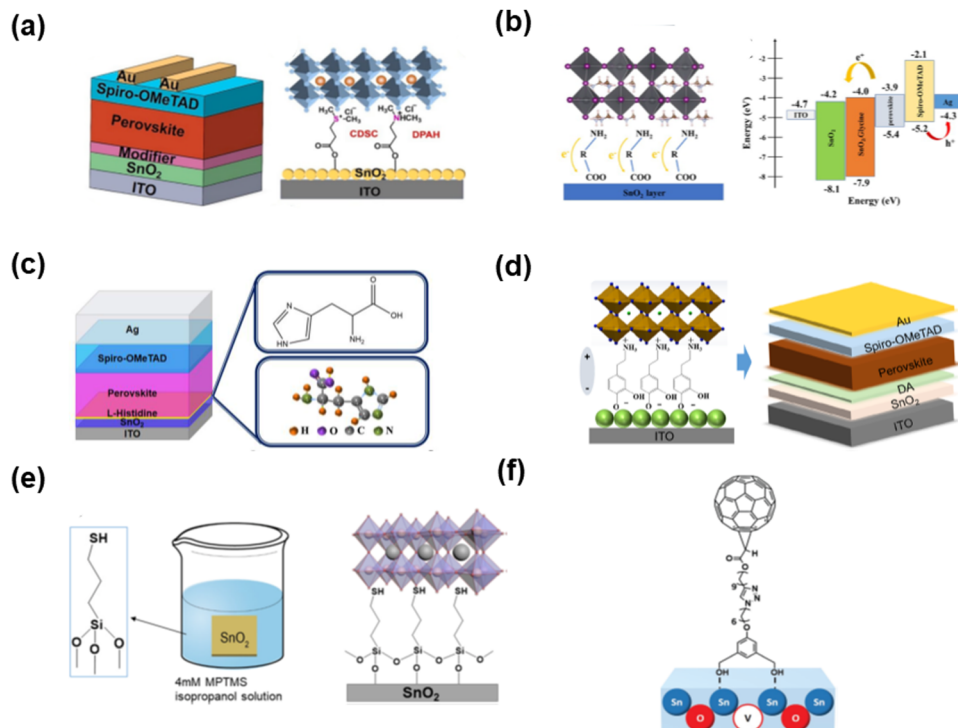
Fig. 16   SAMs in SnO_2-based perovskite solar cells: (a) sulfonium salt-based SAMs. Reproduced with permission.[98] Copyright 2022, Elsevier B.V. (b) Amino acid SAMs. Reproduced with permission.[99] Copyright 2020, Elsevier B.V. (c) Histidine-based ammonia acid (L-His) self-assembled on SnO_2. Reproduced with permission.[100] Copyright 2022, Elsevier B.V. (d) Dopamine SAMs. Reproduced with permission.[101] Copyright 2018, the American Chemical Society. (e) Thiol silane SAMs with cross-linker on SnO_2. Reproduced with permission.[102] Copyright 2021, Wiley-VCH Verlag GmbH & Co. KGaA, Weinheim. (f) Fullerene derivative SAMs in SnO_2. Reproduced with permission.[103] Copyright 2018, The Royal Chemical Society.

(Fig. 16(b)) on SnO_2 to adjust the lattice mismatch at the SnO_2/perovskite interface, and then reduce the interfacial stress. In addition, the end group of ammonia acid can link the SnO_2 with the perovskite film through hydrogen-bonding or electrostatic interactions. Yang and co-authors[100] reported the preparation of another ammonia acid (L-His, Fig. 16(c)) SAM on SnO_2 ETL to improve the crystal quality of the perovskite film. The conductivity of the SnO_2 ETL improved since the carboxyl groups in L-His coordinated with the tin ion in SnO_2 and filled the oxygen vacancy. A dopamine (DA, Fig. 16(d)) SAM was deposited on the top of the SnO_2 electron transporting layer (ETL) to modify the SnO_2/perovskite interface, and then improve the electron extraction and reduce the charge recombination.[101] Zhang and co-authors[102] reported a thiol silane (MPTMS, Fig. 16(e)) SAM to modify the interface between the SnO_2 layer and perovskite film to realize fully air-processed PSCs. The MPTMS SAM interlayer could slow down the crystal growth of the perovskite and smooth the surface of the SnO_2 ETL, which could induce a high-quality perovskite absorber with a champion PCE of over 20%. Zhan and co-authors[103] designed a fullerene derivative (Fig. 16(f)) to anchor on the surface of SnO_2, which could efficiently passivate the oxygen-vacancy-related defects and enhance the extraction rate of the charge carriers. Consequently, the fullerene derivative-modified SnO_2 could achieve a PCE of 21.3%. According to the progress of SnO_2-based devices, it can be found that SAMs can significantly

reduce the defects in SnO_2, and thus the charge recombination. However, it should be noted that the interaction between the terminal group of SAMs and Pb^{2+} is vital for forming high-quality perovskite films. Thus, both factors (SAMs interaction with SnO_2 or Pb^{2+}) should be considered in the design of molecules for these devices.

6.4   SAMs as interfacial modification layers for ZnO-based PSCs

Besides the above-mentioned SAM-modification in the widely used SnO_2 and TiO_2, a similar strategy was also reported in ZnO-based ETLs in PSCs.[104,105] ZnO is an ETL with high electron mobility and low processing temperature. However, the instability of ZnO-based devices is still an issue to be solved because of the proton-transfer reactions between ZnO with the perovskite precursors.[106] Vaynzof and co-authors[107] reported the use of fullerene SAMs (PCBA, Fig. 17(a)) to modify the ZnO/ZnCsO/ZnLiO ETL to enhance the electron extraction with a PCE of up to 18% and improved stability. Zuo et al.[108] developed 3-aminopropanioc acid (C3-SAM, Fig. 17(b)) to modify the ZnO substrate, which could tune the crystallinity and the morphology of the perovskite film with a reduced density of pin-holes and traps. In addition, the work function of the cathode was better aligned with the CB of the perovskite for efficient charge extraction and electronic coupling. Consequently, the performance of the PSC remarkably increased
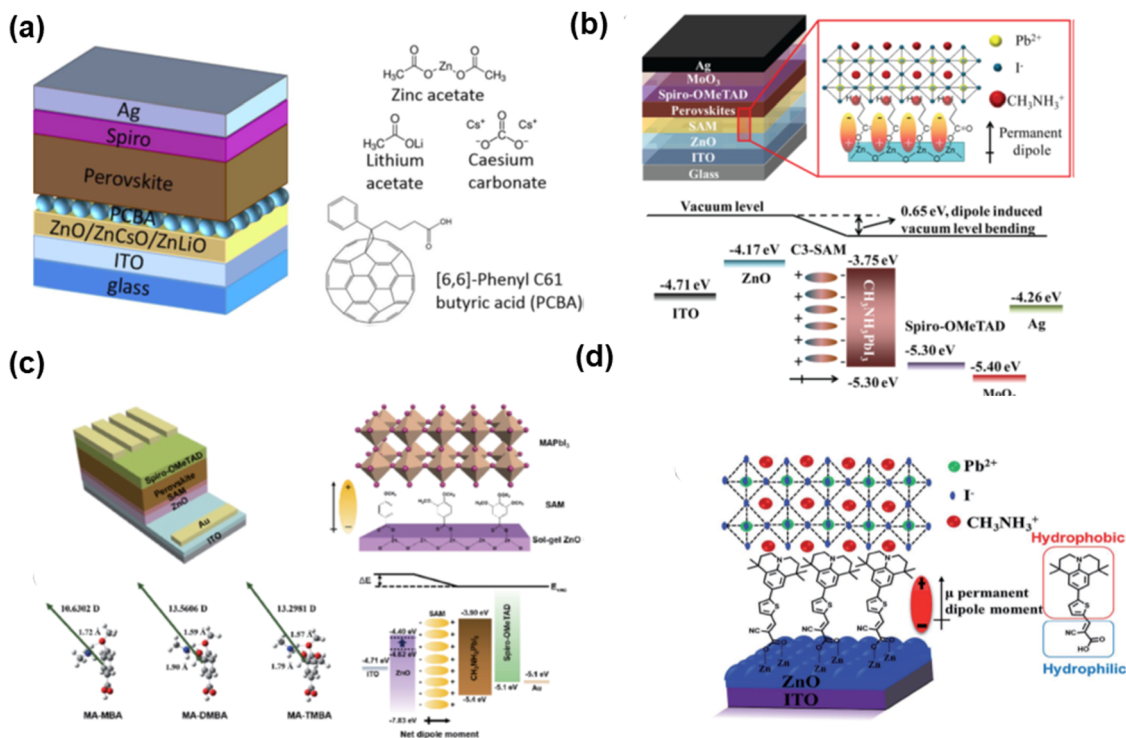
Fig. 17 SAMs in ZnO-based perovskite solar cells: (a) PCBA-based SAMs in ZnO-based device. Reproduced with permission.[107] Copyright 2017, Elsevier B.V. (b) 3-Aminopropanioc acid-based SAMs in ZnO-based device. Reproduced with permission.[108] Copyright 2015, the American Chemical Society. (c) Benzoic acid derivative-based SAMs with various substituted groups in ZnO-based devices. Reproduced with permission.[109] Copyright 2020, The Royal Chemical Society. (d) High dipole moment SAMs with push–pull structure in ZnO-based devices. Reproduced with permission.[110] Copyright 2018, Wiley-VCH Verlag GmbH & Co. KGaA, Weinheim.

from 11.96% to 15.67%. Kim and co-authors[109] designed methoxybenzoic acid-based SAMs (Fig. 17(c)) for adjusting the work function of the ZnO ETL. Specifically, 3,4,5-trimethoxy-benzoic acid (TMBA) with a strong dipole moment could largely shift the work function and enhance the built-in voltage of the device, which resulted in improved electron transfer from the active layer to the ETL and a higher open-circuit voltage. Jang and co-authors[110] designed and synthesized two SAMs (T2CA and JTCA, Fig. 17(d)) with high dipole moments and hydrophobicity, which could effectively improve the quality of the perovskite film and enhance the charge extraction. The JTCA SAM-modified ZnO-based PSCs achieved a PCE of 18.82%. According to the reports on ZnO in PSCs, it is known that the performance of ZnO based-devices is still lower than that of TiO2- and SnO2-based devices. In this case, after treatment with SAMs, the performance and stability of ZnO-based devices can be improved.

The comprehensive photovoltaic parameters of SAMs as interfacial modification layers for n-type metal oxides (TiO2, SnO2 and ZnO) are shown in Table 5. It can be concluded that amino acid- or fullerene-based SAMs are widely applied in n-type metal oxide-based devices, which can effectively passivate the defects (oxygen vacancies) in metal oxide-based ETLs to reduce the hysteresis and improve the stability of PSCs. Moreover, the electron transfer rate from the perovskite to the ETLs is enhanced and the charge recombination is reduced after the modification of metal oxides with SAMs. Regarding the progress of metal oxide-based ETLs, the SAMs containing fullerenes exhibit better passivating ability and performance, especially in TiO2-based devices.

7. SAMs as interfacial modification layers for perovskite films

The above-mentioned progress on SAMs as interfacial layers for NiOx−, TiO2−, SnO2− and ZnO-based CTLs is impressive. Due to the existence of functional groups in SAMs, they can also act as the passivating layer on top of the perovskite film to improve the stability of the device. To clarify the difference between SAMs and small/polymer molecules as interfacial layers in PSCs, the anchoring group and thickness of the interfacial layers are two important factors to distinguish them. If there is no anchoring group in small/polymer molecules, they can be regarded as a passivation layer or interface modifier by organic molecules. However, when there are anchoring groups of organic molecules that can attach to surface of metal oxides or the perovskite film through chemical binding with an ultrathin film, they should be regarded as interfacial layers by SAMs. Wolff et al.[111] used perfluorinated halogenated SAMs (Fig. 18(a)) to passivate the top surface of a perovskite film. It was found that the perovskite surface with I-terminated

Table 5 The SAMs as interfacial modification layers for n-type metal oxides

SAMs	Perovskite	V_{oc} (V)	J_{sc} (mA cm^{-2})	FF (%)	PCE (%)	Ref.
TiO$_2$(c)/C$_{60}$-SAM	CH$_3$NH$_3$PbI$_{3-x}$Cl$_x$	1.04	22.1	75	17.3	84
TiO$_2$(m)/C$_{60}$-SAM	CH$_3$NH$_3$PbI$_{3-x}$Cl$_x$	0.84	19.6	72	11.7	85
TiO$_2$(m)/HOCO–R–NH$_3$I	MAPbI$_3$	1.00	19.2	62	12.0	86
TiO$_2$(m)/Silane-SAM	MAPbI$_3$	0.873	19.51	75	12.7	87
TiO$_2$(c)/C-PCBA	CsFAMA	1.148	26.1	82.8	24.81	88
TiO$_2$(m)/CBA	CsFAMA	1.101	24.25	79.81	21.35	89
TiO$_2$(m)/MBA	CsFAMA	1.094	23.87	79.29	20.73	89
TiO$_2$(m)/β-ALA	CsFAMA	1.096	23.10	76.69	19.43	89
TiO$_2$(m)/4-PA	MAPbI$_3$	1.06	23.15	77	18.90	90
TiO$_2$(m)/HOOC–Ph–SH	MAPbI$_3$	1.02	20.66	66.54	14.11	91
TiO$_2$(m)/HOOC–(CH$_2$)$_2$–SH	MAPbI$_3$	1.01	20.08	66.38	13.45	91
TiO$_2$(m)/HOOC–(CH$_2$)$_6$–SH	MAPbI$_3$	0.98	19.04	63.18	11.80	91
TiO$_2$(m)/HOOC–(CH$_2$)$_{11}$–SH	MAPbI$_3$	0.97	18.28	57.71	10.32	91
TiO$_2$(m)/IMPA	MAPbI$_3$	0.96	23.59	67.15	15.21	92
TiO$_2$(m)/IBPA	MAPbI$_3$	0.94	21.75	67.62	13.83	92
TiO$_2$(m)/IHPA	MAPbI$_3$	0.92	20.64	58.13	11.04	92
TiO$_2$(m)/BPA	MAPbI$_3$	0.90	20.55	63	11.65	92
TiO$_2$(m)/APPA	MAPbI$_3$	0.94	22.93	64.27	13.85	92
TiO$_2$(m)/TFBPA	MAPbI$_3$	0.98	23.24	70.67	16.09	92
SnO$_2$/H-SAM	Cs$_{0.05}$(FA$_{0.85}$MA$_{0.15}$)$_{0.95}$Pb(I$_{0.85}$Br$_{0.15}$)$_3$	1.143	23.18	76.2	20.19	95
SnO$_2$/I-SAM	Cs$_{0.05}$(FA$_{0.85}$MA$_{0.15}$)$_{0.95}$Pb(I$_{0.85}$Br$_{0.15}$)$_3$	1.185	23.26	77.8	21.44	95
SnO$_2$/S	MAPbI$_3$	1.06	22.61	76.85	18.41	96
SnO$_2$/BA-SAM	MAPbI$_3$	1.11	21.88	74.6	18.11	97
SnO$_2$/PA-SAM	MAPbI$_3$	1.10	22.03	77.4	18.77	97
SnO$_2$/CBA	MAPbI$_3$	1.08	21.66	78.1	18.27	97
SnO$_2$/ABA	MAPbI$_3$	1.04	22.00	72.1	16.50	97
SnO$_2$/C3-SAM	MAPbI$_3$	1.08	21.48	73.8	17.11	97
SnO$_2$/DPAH	RbCsFA	1.143	23.11	81.3	21.44	98
SnO$_2$/CDSC	RbCsFA	1.163	23.18	82.5	22.22	98
SnO$_2$/glycine	Cs$_{0.05}$MA$_y$FA$_{0.95-y}$PbI$_{3-x}$Cl$_x$	1.10	24.15	78	20.68	99
SnO$_2$/L-His	MAPbI$_3$	1.16	22.74	79.76	21.04	100
SnO$_2$/DA	MAPbI$_3$	1.05	21.80	73.9	16.87	101
SnO$_2$/MPTMS	(FAPbI$_3$)$_x$(MAPbBr$_3$)$_{1-x}$	1.112	23.60	76.32	20.03	102
SnO$_2$/C9	(FAPbI$_3$)$_x$(MAPbBr$_3$)$_{1-x}$	1.12	24.1	78.9	21.3	103
ZnLiO/PCBA	MAPbI$_3$	1.03	19.2	82.1	16.2	107
ZnO/C3-SAM	MAPbI$_3$	1.07	22.51	65	15.67	108
ZnO/MBA	MAPbI$_3$	0.98	20.95	61.18	12.60	109
ZnO/DMBA	MAPbI$_3$	1.01	21.13	60.54	12.97	109
ZnO/TMBA	MAPbI$_3$	1.05	21.38	60.96	13.75	109
ZnO/T2CA	MAPbI$_3$	1.09	21.34	0.73	17.07	110
ZnO/JTCA	MAPbI$_3$	1.13	21.72	0.76	18.82	110

fluorocarbons increased the V_{oc} up to 1.18 V without sacrificing other photovoltaic parameters. Subsequently, the SAM-modified perovskite devices could achieve a PCE of over 21%. Moreover, the champion device exhibited a stable maximum power point operation at 85 °C for more than 250 h and maintained about 95% of its initial PCE after storage in humid air under ambient conditions over 3000 h. Bai et al.[112] reported the preparation of a water-resistant cross-linkable silane-functionalized fullerene ETL (Fig. 18(b)) to improve the stability of inverted PSCs under moisture. With the introduction of molecular (methylammonium iodide) doping in the cross-linked silane-modified fullerene layer, its conductivity improved. The combination of crosslinking and doping can simultaneously improve the PCE and stability of PSCs in an ambient environment without encapsulation. Guo et al.[113] proposed a cholesterol derivative self-assembly strategy to construct crosslinked and compact membranes throughout perovskite films. These supramolecular membranes (Fig. 18(c)) could act as a robust protection layer against harsh operational conditions. In addition, the formed SAMs could effectively passivate the defects from the surface toward the inner grain boundaries. The SAM (CDCA-TMA)-modified PSCs exhibited a PCE of 23.34% with an impressive V_{oc} of 1.164 V. The unencapsulated devices retained 92% of their initial efficiencies after 1600 h storage under ambient conditions. Additionally, the PCE remained almost unchanged after heating at 85 °C for 500 h in a nitrogen atmosphere, showing significantly improved stability. A similar case was reported by Zhang et al.,[114] who exploited an insulating alkyl chain (C$_{12}$-silane, Fig. 18(d)) to adsorb on the top surface of the perovskite layer through the interaction of hydrogen bonding between Si–OH and I$^-$, leaving the long alkyl chain terminal group out from the surface. Further analysis indicated that the formed insulating barrier layer with the long alkyl chain can reduce the interfacial charge recombination and make the perovskite surface to be more hydrophobic toward moisture. These results indicated that the deposited SAMs on the top of the perovskite layer can effectively passivate the defects on the surface of the perovskite film and increase the hydrophobic characteristics of its surface, which can contribute to improving the performance and stability of the device.
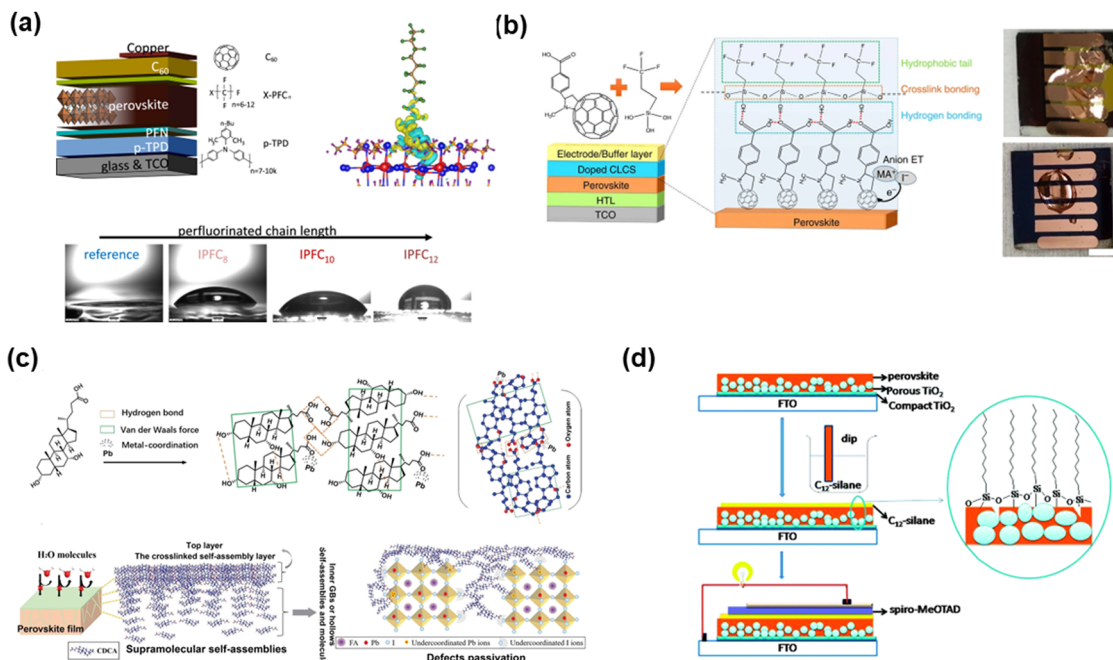
Fig. 18 SAMs on the top of perovskite film: (a) perfluorinated aliphatic carbon chains with iodine (X-PFC$_n$). Reproduced with permission.[111] Copyright 2020, the American Chemical Society. (b) Cross-linkable silane-functionalized fullerene SAMs. Reproduced with permission.[112] Copyright 2016, Nature. (c) Cholesterol derivative SAMs. Reproduced with permission.[113] Copyright 2022, Wiley-VCH Verlag GmbH & Co. KGaA, Weinheim. (d) C$_{12}$-silane SAMs. Reproduced with permission.[114] Copyright 2015, The Royal Chemical Society.

The various dipole moments of SAMs on the top of the perovskite layer can influence the surface potential and adjust the energy level of the perovskite film. As shown in Fig. 19(a), Wang et al.[115] employed 4-chlorobenzoic acid (4ClBA) to form an SAM layer on the surface of perovskite film. Besides the function of passivating perovskite surface defects, 4ClBA with dipole moment can tune the energy level alignment and form a larger energetic driving force for hole extraction. The V_{oc} of the device increased from 1.08 to 1.16 V with a PCE of 21%. Kong and co-authors[116] used tetrabutylammonium chloride (TBAC, Fig. 19(b)) to self-assemble on the surface of the perovskite film. Because of the strong interface dipole pointing outward of the surface of the perovskite, the formed built-in electric field could enhance the transfer of holes. The PSCs self-assembled with TABC could achieve a PCE of 23.50% with an FF of 0.82. To further discuss the effect of SAMs with various dipole moments on the WF of perovskite films, Han and co-authors[117] reported the preparation of three SAMs (CA1, CA2 and CA3) with different dipole moments to self-assemble on the surface of the perovskite film, which could induce the formation of an extra electric field and is consistent with the local built-in electric field (Fig. 19(c)). The larger dipole moment could induce a stronger extra electric field to enhance the electron collection. Consequently, CA-3 with the highest dipole moment attained a PCE of 21.4% with a voltage of 1.155 V.

To discuss the passivating ability of various SAMs on the surface of perovskite films, Han and co-authors[118] designed three D–π–A-structured organic molecules (SP1, SP2 and SP3) with various electron density distributions to anchor on the perovskite film (Fig. 19(d)). The results indicated that the strong electron-donating N,N-dibutylaminophenyl unit of SP3 notably increased the electron density on the anchoring group and make it much more electron-rich, which can provide better conditions for coordination with the under-coordinated Pb^{2+} defects. SP3 with strong passivating ability could achieve a PCE of 20.43% with an improvement in the V_{oc} to 1.146 V. According to the above-mentioned progress of SAMs on the top of the perovskite film, as summarized in Table 6, SAMs with a dipole moment are very important for adjusting the energy level on the surface of the perovskite layer and enhancing the passivating ability.

8. The application of SAMs in large-area devices or modules

Besides the above-mentioned application of SAMs in improving small-area devices, SAMs also have very promising applications in large-area PSCs because of their uniform film formation and low temperature processes. Especially in p–i–n-based PSCs, the ultrathin film of the HTLs restricts its large-area deposition by doctor-blade coating. However, SAMs are suitable for the deposition of an ultrathin film on the conductive substrate on a large scale. Unger and co-authors[119] used 2PACz SAMs (Fig. 20(a)) to prepare high-quality HTLs on ITO electrodes for inverted PSCs. The optimized devices maintained about 80% of their initial average PCE during the maximum power point (MPP) tracking for > 700 h. A PCE of 19.4% was achieved for a
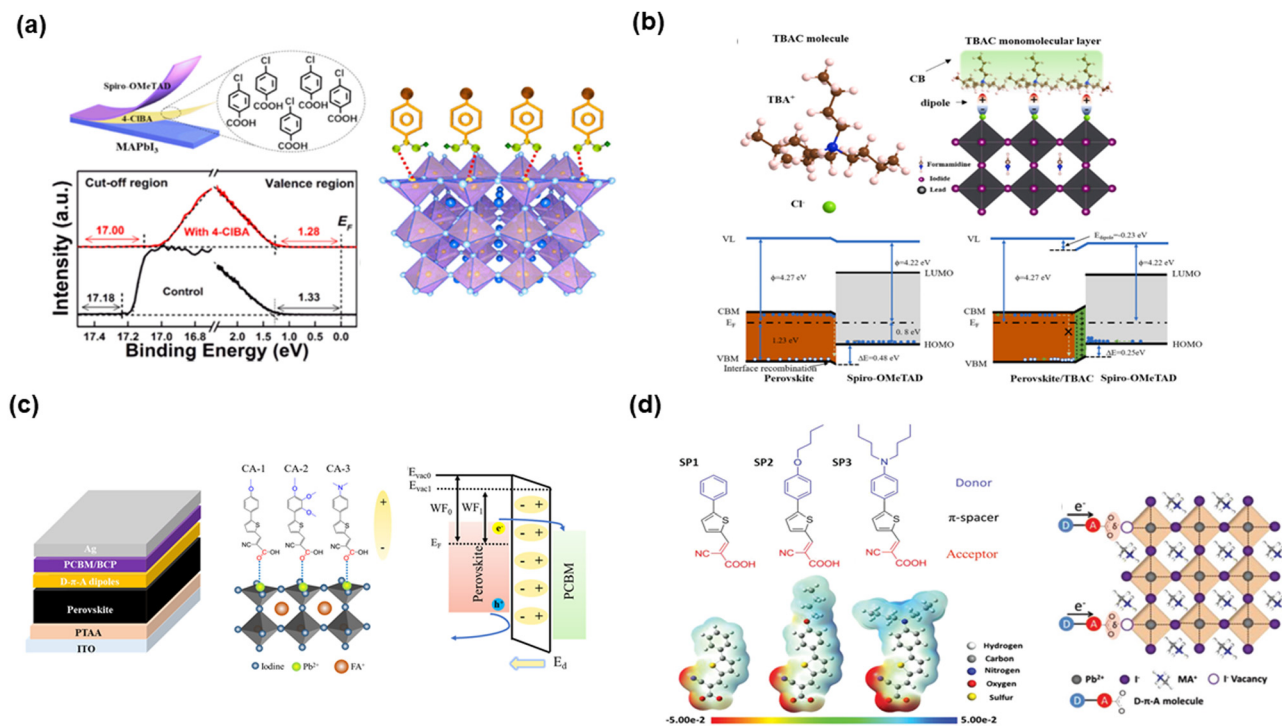
Fig. 19 SAMs on the top of perovskite film: (a) 4-chlorobenzoic acid (4ClBA) anchored on the perovskite layer. Reproduced with permission.[115] Copyright 2022, Elsevier B.V. (b) Tetrabutylammonium chloride (TBAC) with large dipole moment on perovskite layer. Reproduced with permission.[116] Copyright 2022, Elsevier B.V. (c) Three organic molecules with various dipole moments on the perovskite layer. Reproduced with permission.[117] Copyright 2021, The Royal Chemical Society. (d) Organic molecules with D−π−A structured on the perovskite layer. Reproduced with permission.[118] Copyright 2019, Wiley-VCH Verlag GmbH & Co. KGaA, Weinheim.

2.2 cm^2 mini-module. Jen and co-authors[120] used MeO-2PACz-based SAMs (Fig. 20(b)) as HTLs to prepare a module with an aperture area of 18 cm^2. Also, the module could achieve a PCE of 14.13%. Zhu and co-authors[121] reported the synergistic co-adsorption of a hydrophilic ammonium salt CA-Br (Fig. 20(c)) with a triphenylamine derivative-SAM to obtain scalable and wettable HTLs for inverted PSCs. The mixed self-assembled route not only enabled the formation of ultrathin HTLs with high uniformity but also eliminated the non-wetting problem to facilitate the growth of large-area perovskite films with 100%

coverage. Moreover, the incorporation of CA-Br in SAMs could maintain a high quality of electronic connection via the passivation of the cation vacancies. Consequently, a high PCE of 17.49% was achieved for small-area PSCs (1.02 cm^2), and the module with an aperture area of 36 cm^2 showed a PCE of 12.67%. Additionally, Zuo et al.[122] reported the use of 3-amino-propanoic acid as a self-assembled monolayer (C3-SAM, Fig. 20(d)) to modify a (PEDOT:PSS)-based HTL for improving the crystallinity and coverage of the perovskite film, resulting in a much smoother perovskite surface morphology together with

Table 6 SAMs as interfacial modification layers on the top of perovskite films

| SAMs	Perovskite	V_{oc} (V)	J_{sc} (mA cm^{-2})	FF (%)	PCE (%)	Ref.
IPFC8	$CsI_{0.05}[FA_{0.85}MA_{0.15}Pb(I_{0.85}Br_{0.15})_3]_{0.95}$	1.11	22.80	79	20	111
IPFC10	$CsI_{0.05}[FA_{0.85}MA_{0.15}Pb(I_{0.85}Br_{0.15})_3]_{0.95}$	1.18	22.28	81	21.3	111
IPFC12	$CsI_{0.05}[FA_{0.85}MA_{0.15}Pb(I_{0.85}Br_{0.15})_3]_{0.95}$	1.16	23.20	78	21	111
CLCS	$MAPbI_3$	1.06	22.7	80.0	19.3	112
CDCA-TMN	$FA_{0.97}MA_{0.03}PbI_3$	1.164	25.58	78.94	23.34	113
CDCA	$FA_{0.97}MA_{0.03}PbI_3$	1.170	25.58	75.41	13.75	113
CHOL	$FA_{0.97}MA_{0.03}PbI_3$	1.112	24.93	78.94	21.87	113
C12-silane	$MAPbI_3$	0.959	20.23	67.7	13.74	114
4-ClBA	$MAPbI_3$	1.16	22.86	79	21	115
TBAC	$FAPbI_3$	1.15	24.80	82.90	23.50	116
SP1	$MAPbI_3$	1.075	22.53	77.42	18.75	117
SP2	$MAPbI_3$	1.094	22.63	77.82	19.27	117
SP3	$MAPbI_3$	1.146	22.69	78.55	20.43	117
CA-1	$MAPbI_3$	1.109	21.9	80.8	19.64	118
CA-2	$MAPbI_3$	1.118	22.1	82	20.3	118
CA-3	$MAPbI_3$	1.155	22.28	83.07	21.4	118
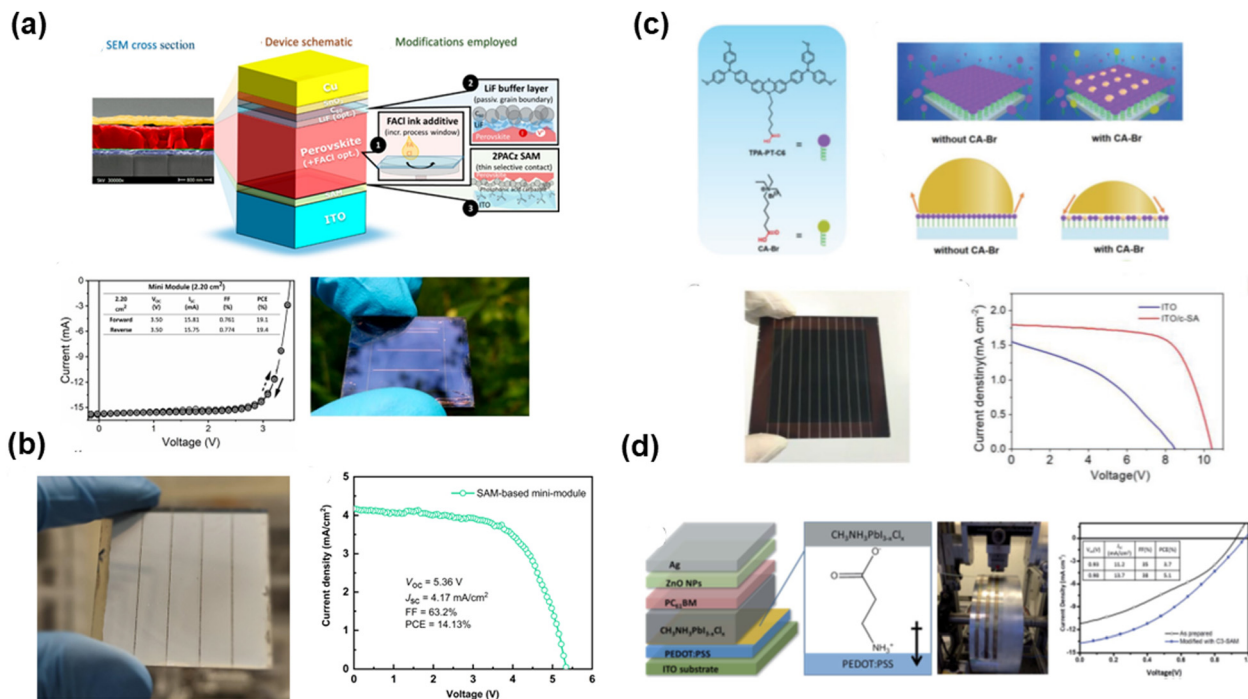
Fig. 20 SAMs for large-area perovskite solar cells: (a) carbazole SAMs (2PACz) with an area of 2.20 cm^2. Reproduced with permission.[119] Copyright 2021, the American Chemical Society. (b) MeO-2PACz SAMs with an area of 18 cm^2. Reproduced with permission.[120] Copyright 2022, Tsinghua University Press. (c) Two SAMs of hydrophilic ammonium salt and triphenylamine derivatives. Reproduced with permission.[121] Copyright 2020, Wiley-VCH Verlag GmbH & Co. KGaA, Weinheim. (d) 3-Aminopropanoic acid SAM-modified PEDOT:PSS. Reproduced with permission.[122] Copyright 2015, The Royal Chemical Society.

an increase in PCE from 9.7% to 11.6%. They further used a roll-to-roll method to prepare large-area flexible PSCs. The C3-SAM-modified devices increased the PCE from 3.7% to 5.1%. The SAMs displayed ability to achieve large-area PSC modules and the strategy of synergistic SAMs can adjust the wettability for the large-area deposition of perovskite films. However, the PCE of the large-area PSC module is still needs to be further optimized due to the sub-optimized uniformity of both the SAMs and perovskites. To further improve the performance of the PSC module, the wettability and dipole moment should be carefully adjusted to satisfy the large-area process and energy alignment, respectively. Sometimes, it is difficult for one type of SAM to maintain both characters. Thus, synergistic SAMs with binary organic molecules are promising candidates for further improving the performance of PSC modules.

9. Conclusion and perspective

In this review, we introduced the concept of SAMs and summarized their application in PSCs for addressing the current challenge associated with PSCs. Firstly, we introduced the SAMs as the HTL for inverted PSCs. It was found that carbazole-based SAMs achieved good performances as HTLs in inverted PSCs. In addition, various alkyl chain lengths in the linker of carbazole-based SAMs can produce tunnel barriers with different widths. In the case of non-conjugated linkers, the longer the

alkyl chain, the larger the resistance formed at the interface. The conjugated linker in SAMs shows fast hole transfer and good stability. Besides carbazole-based SAMs, triphenylamine and phenothiazine derivative-based SAMs have also shown ability as HTLs in inverted PSCs. Naphthalene-imide and fullerene derivative-based SAMs can be regarded as ETLs in n–i–p-based PSCs with low temperature processes. For the modification layers, the SAMs can effectively passivate the defects and adjust the energy level at the interface of the metal oxide/perovskite. More importantly, SAMs have also shown potential in the PSC module.

According to the content reviewed above, some strategies can be summarized for designing novel SAMs in the future. SAMs as HTLs or ETLs in PSCs: the dipole moments of the SAM molecules should be considered depending on the device configuration and types of interlayers. Through molecular design, optimal charge extraction by adjusting the energy barrier can be realized. Given that the WF of CTLs can be regulated by surface dipoles, SAM modification is an effective way to adjust the energy levels at these interfaces in PSCs. In addition to charge extraction, the V_{oc} is also related to the WF of CTLs, which changes the built-in potential in PSCs. The direction of the dipole moments in SAMs is vital to realize a high performance. In the case of HTL-based SAMs in inverted PSCs, the dipole moment should point toward the substrate. However, for ETL-based SAMs, the direction of dipole moment should be the opposite. According to the progress of SAMs for

HTLs in inverted PSCs, some conclusions can be made for the future design of SAMs. For the terminal group of SAMs, strong electron-donating groups are more attractive, such as carbazole, triphenylamine and phenoxazine derivatives. In addition, to finely tune the work function and passivate the perovskite film, halogenated terminal groups are recommended. For the linker group, although non-conjugated alkyl linkers have achieved significant progress, their hole-transporting capability and stability are still lower than that of conjugated linkers. Thus, to further improve the performance of SAM-based device, more conjugated linkers can be considered. For the anchoring groups, various anchoring group-based SAMs have been tried in PSCs. It seems that phosphonic acid and cyanoacetic acid are good candidates as the anchoring groups because of their fast adsorption dynamics and strong bonding strength, which can increase the coverage and stability of SAMs on the conductive substrate.

SAMs as interfacial modifying layer for metal oxide in PSCs: regarding the interfacial modified layers, the main role of SAMs is to passivate the defects in the metal oxide-based CTLs. In addition, the terminal group of SAMs should have a group to interact with the perovskite film to adjust its morphology (amino acid, organic silane, *etc.*).

Finally, we should understand that there are different standards for SAM application in pure charge transport layers and modifying layers. To prepare high-performance PSCs, the following standards should be considered for selecting SAMs: (1) the direction of the dipole moment should be pointed toward the ITO substrate for the SAMs as the HTL or interfacial layer for p-type metal oxides (NiO_x). (2) For SAMs as the ETL or interfacial layer for n-type metal oxides (TiO_2, SnO_2 and ZnO), the direction of the dipole moment should point away from the ITO substrate. (3) The fine adjustment of the energy level for SAMs can be achieved through the substitution of the terminal group to match the energy level with the perovskite film. Consequently, more work is required on molecular design and deposition methods to solve these challenges. For example, more novel SAMs are required to compare the characteristics of dipole moments and energy levels. For further application in large-area PSC modules, SAMs should have suitable wettability on the perovskite film. More importantly, the UV stability of SAMs should be considered for molecular design. For example, the concept of excellent UV stability can be applied to the modification of SAMs. In addition, more deposition methods should be developed for SAMs on the conductive substrate besides the solution process, such as vacuum evaporation. In summary, we hope that this review will provide useful insight for the research community to further improve the performance of SAM-based PSCs and modules. This cost-efficient methodology should lead to the practical application of PSCs in daily life and occupy a significant place in the future energy market.

Conflicts of interest

There are no conflicts to declare.

Acknowledgements

References

1 A. Kojima, K. Teshima, Y. Shirai and T. Miyasaka, Organometal halide perovskites as visible-light sensitizers for photovoltaic cells, *J. Am. Chem. Soc.*, 2009, **131**, 6050–6051.

2 H.-S. Kim, C.-R. Lee, J.-H. Im, K.-B. Lee, T. Moehl, A. Marchioro, S.-J. Moon, R. Humphry-Baker, J.-H. Yum, J. E. Moser, M. Grätzel and N.-G. Park, Lead iodide perovskite sensitized all-solid-state submicron thin film mesoscopic solar cell with efficiency exceeding 9%, *Sci. Rep.*, 2012, **2**, 591.

3 M. M. Lee, J. Teuscher, T. Miyasaka, T. N. Murakami and H. J. Snaith, Efficient hybrid solar cells based on meso-superstructured organometal halide perovskites, *Science*, 2012, **338**, 643–647.

4 National Renewable Energy Laboratory, Best Research-Cell Efficiency Chart, **https://www.nrel.gov/pv/cell-efficiency.html**.

5 M. A. Green and A. Ho-Baillie, Perovskite solar cells: the birth of a new era in photovoltaics, *ACS Energy Lett.*, 2017, **2**, 822–830.

6 J. Seo, J. H. Noh and S. I. Seok, Rational strategies for efficient perovskite solar cells, *Acc. Chem. Res.*, 2016, **49**, 562–572.

7 J.-P. Correa-Baena, M. Saliba, T. Buonassisi, M. Grätzel, A. Abate, W. Tress and A. Hagfeldt, Promises and challenges of perovskite solar cells, *Science*, 2017, **358**, 739–744.

8 Y. Rong, Y. Hu, A. Mei, H. Tan, M. I. Saidaminov, S. I. Seok, M. D. McGehee, E. H. Sargent and H. Han, Challenges for commercializing perovskite solar cells, *Science*, 2018, **361**, eaat8235.

9 M. A. Green, A. Ho-Baillie and H. J. Snaith, The emergence of perovskite solar cells, *Nat. Photonics*, 2014, **8**, 506–514.

10 F. Gao, Y. Zhao, X. Zhang and J. You, Recent progresses on defect passivation toward efficient perovskite solar cells, *Adv. Energy Mater.*, 2020, **10**, 1902650.

11 F. Ali, C. Roldán-Carmona, M. Sohail and M. K. Nazeeruddin, Applications of self-assembled monolayers for perovskite solar cells interface engineering to address efficiency and stability, *Adv. Energy Mater.*, 2020, **10**, 2002989.

12 A. K. Jena, A. Kulkarni and T. Miyasaka, Halide perovskite photovoltaics: background, status, and future prospects, *Chem. Rev.*, 2019, **119**, 3036–3103.

13 J. Y. Kim, J.-W. Lee, H. S. Jung, H. Shin and N.-G. Park, High-efficiency perovskite solar cells, *Chem. Rev.*, 2020, **120**, 7867–7918.

14 U. Bach, D. Lupo, P. Comte, J. E. Moser, F. Weissörtel, J. Salbeck, H. Spreitzer and M. Grätzel, Solid-state dye-

sensitized mesoporous TiO_2 solar cells with high photon-to-electron conversion efficiencies, *Nature*, 1998, **395**, 583–585.

15 M. Liu, M. B. Johnston and H. J. Snaith, Efficient planar heterojunction perovskite solar cells by vapour deposition, *Nature*, 2013, **501**, 395–398.

16 L. Meng, J. You, T.-F. Guo and Y. Yang, Recent advances in the inverted planar structure of perovskite solar cells, *Acc. Chem. Res.*, 2016, **49**, 155–165.

17 D. Mandler and S. Kraus-Ophir, Self-assembled mono-layers (SAMs) for electrochemical sensing, *J. Solid State Electrochem.*, 2011, **15**, 1535.

18 J. J. Gooding, F. Mearns, W. Yang and J. Liu, Self-assembled monolayers into the 21st century: recent advances and applications, *Electroanalysis*, 2003, **15**, 81–96.

19 A. Badia, R. B. Lennox and L. Reven, A dynamic view of self-assembled monolayers, *Acc. Chem. Res.*, 2000, **33**, 475–481.

20 J. C. Love, L. A. Estroff, J. K. Kriebel, R. G. Nuzzo and G. M. Whitesides, Self-assembled monolayers of thiolates on metals as a form of nanotechnology, *Chem. Rev.*, 2005, **105**, 1103–1170.

21 A. Ulman, Formation and structure of self-assembled monolayers, *Chem. Rev.*, 1996, **96**, 1533–1554.

22 S. P. Pujari, L. Scheres, A. T. M. Marcelis and H. Zuilhof, Covalent surface modification of oxide surfaces, *Angew. Chem., Int. Ed.*, 2014, **53**, 6322–6356.

23 R. W. Zehner, B. F. Parsons, R. P. Hsung and L. R. Sita, Tuning the Work Function of Gold with Self-Assembled Monolayers Derived from $X–[C_6H_4–C{\equiv}C–]_nC_6H_4–SH$ (n = 0, 1, 2; X = H, F, CH_3, CF_3, and OCH_3), *Langmuir*, 1999, **15**, 1121–1127.

24 B. de Boer, A. Hadipour, M. M. Mandoc, T. van Woudenbergh and P. W. M. Blom, Tuning of Metal Work Functions with Self-Assembled Monolayers, *Adv. Mater.*, 2005, **17**, 621–625.

25 W. Yan, S. Ye, Y. Li, W. Sun, H. Rao, Z. Liu, Z. Bian and C. Huang, Hole-transporting materials in inverted planar perovskite solar cells, *Adv. Energy Mater.*, 2016, **6**, 1600474.

26 Y. Xia and S. Dai, Review on applications of PEDOTs and PEDOT:PSS in perovskite solar cells, *J. Mater. Sci. Mater.*, 2021, **32**, 12746–12757.

27 D. Di Girolamo, F. Di Giacomo, F. Matteocci, A. G. Marrani, D. Dini and A. Abate, Progress, highlights and perspectives on NiO in perovskite photovoltaics, *Chem. Sci.*, 2020, **11**, 7746–7759.

28 M. Li, Y. Xie, F. R. Lin, Z. Li, S. Yang and A. K. Y. Jen, Self-assembled monolayers as emerging hole-selective layers enable high-performance thin-film solar cells, *Innovation*, 2023, **4**, 100369.

29 A. Magomedov, A. Al-Ashouri, E. Kasparavičius, S. Strazdaite, G. Niaura, M. Jošt, T. Malinauskas, S. Albrecht and V. Getautis, Self-assembled hole transporting mono-layer for highly efficient perovskite solar cells, *Adv. Energy Mater.*, 2018, **8**, 1801892.

30 A. Al-Ashouri, A. Magomedov, M. Roß, M. Jošt, M. Talaikis, G. Chistiakova, T. Bertram, J. A. Márquez, E. Köhnen, E. Kasparavičius, S. Levcenco, L. Gil-Escrig, C. J. Hages, R. Schlatmann, B. Rech, T. Malinauskas, T. Unold, C. A. Kaufmann, L. Korte, G. Niaura, V. Getautis and S. Albrecht, Conformal monolayer contacts with lossless interfaces for perovskite single junction and monolithic tandem solar cells, *Energy Environ. Sci.*, 2019, **12**, 3356–3369.

31 A. Farag, T. Feeney, I. M. Hossain, F. Schackmar, P. Fassl, K. Küster, R. Bäuerle, M. A. Ruiz-Preciado, M. Hentschel, D. B. Ritzer, A. Diercks, Y. Li, B. A. Nejand, F. Laufer, R. Singh, U. Starke and U. W. Paetzold, Evaporated self-assembled monolayer hole transport layers: lossless inter-faces in p–i–n perovskite solar cells, *Adv. Energy Mater.*, 2023, 2203982.

32 D. Song, S. Narra, M.-Y. Li, J.-S. Lin and E. W.-G. Diau, Interfacial engineering with a hole-selective self-assembled monolayer for tin perovskite solar cells via a two-step fabrication, *ACS Energy Lett.*, 2021, **6**, 4179–4186.

33 G. Kapil, T. Bessho, Y. Sanehira, S. R. Sahamir, M. Chen, A. K. Baranwal, D. Liu, Y. Sono, D. Hirotani, D. Nomura, K. Nishimura, M. A. Kamarudin, Q. Shen, H. Segawa and S. Hayase, Tin–lead perovskite solar cells fabricated on hole selective monolayers, *ACS Energy Lett.*, 2022, **7**, 966–974.

34 X. Deng, F. Qi, F. Li, S. Wu, F. R. Lin, Z. Zhang, Z. Guan, Z. Yang, C.-S. Lee and A. K.-Y. Jen, Co-assembled mono-layers as hole-selective contact for high-performance inverted perovskite solar cells with optimized recombina-tion loss and long-term stability, *Angew. Chem., Int. Ed.*, 2022, **61**, e202203088.

35 W. Jiang, F. Li, M. Li, F. Qi, F. R. Lin and A. K.-Y. Jen, π-expanded carbazoles as hole-selective self-assembled monolayers for high-performance perovskite solar cells, *Angew. Chem., Int. Ed.*, 2022, **61**, e202213560.

36 A. Al-Ashouri, M. Marčinskas, E. Kasparavičius, T. Malinauskas, A. Palmstrom, V. Getautis, S. Albrecht, M. D. McGehee and A. Magomedov, Wettability improve-ment of a carbazole-based hole-selective monolayer for reproducible perovskite solar cells, *ACS Energy Lett.*, 2023, **8**, 898–900.

37 X. Zheng, Z. Li, Y. Zhang, M. Chen, T. Liu, C. Xiao, D. Gao, J. B. Patel, D. Kuciauskas, A. Magomedov, R. A. Scheidt, X. Wang, S. P. Harvey, Z. Dai, C. Zhang, D. Morales, H. Pruett, B. M. Wieliczka, A. R. Kirmani, N. P. Padture, K. R. Graham, Y. Yan, M. K. Nazeeruddin, M. D. McGehee, Z. Zhu and J. M. Luther, Co-deposition of hole-selective contact and absorber for improving the processability of perovskite solar cells, *Nat. Energy*, 2023, **8**, 462–472.

38 K. Almasabi, X. Zheng, B. Turedi, A. Y. Alsalloum, M. N. Lintangpradipto, J. Yin, L. Gutiérrez-Arzaluz, K. Kotsovos, A. Jamal, I. Gereige, O. F. Mohammed and O. M. Bakr, Hole-transporting self-assembled monolayer enables effi-cient single-crystal perovskite solar cells with enhanced stability, *ACS Energy Lett.*, 2023, **8**, 950–956.

39 I. Levine, A. Al-Ashouri, A. Musiienko, H. Hempel, A. Magomedov, A. Drevilkauskaite, V. Getautis, D. Menzel, K. Hinrichs, T. Unold, S. Albrecht and T. Dittrich, Charge

transfer rates and electron trapping at buried interfaces of perovskite solar cells, *Joule*, 2021, **5**, 2915–2933.

40 I. Levine, S. M. Weber, Y. Feldman, T. Bendikov, H. Cohen, D. Cahen and A. Vilan, Molecular length, monolayer density, and charge transport: lessons from Al–AlO$_x$/Alkyl–Phosphonate/Hg junctions, *Langmuir*, 2012, **28**, 404–415.

41 A. Ullah, K. H. Park, Y. Lee, S. Park, A. B. Faheem, H. D. Nguyen, Y. Siddique, K.-K. Lee, Y. Jo, C.-H. Han, S. Ahn, I. Jeong, S. Cho, B. Kim, Y. S. Park and S. Hong, Versatile hole selective molecules containing a series of heteroatoms as self-assembled monolayers for efficient p–i–n perovskite and organic solar cells, *Adv. Funct. Mater.*, 2022, **32**, 2208793.

42 N. Singh, A. Mohapatra, C.-W. Chu and Y.-T. Tao, Modulation of work function of ITO by self-assembled monolayer and its effect on device characteristics of inverted perovskite solar cells, *Org. Electron.*, 2021, **98**, 106297.

43 R. Guo, X. Zhang, X. Zheng, L. Li, M. Li, Y. Zhao, S. Zhang, L. Luo, S. You, W. Li, Z. Gong, R. Huang, Y. Cui, Y. Rong, H. Zeng and X. Li, Tailoring multifunctional self-assembled hole transporting molecules for highly efficient and stable inverted perovskite solar cells, *Adv. Funct. Mater.*, 2023, 2211955.

44 E. Li, C. Liu, H. Lin, X. Xu, S. Liu, S. Zhang, M. Yu, X.-M. Cao, Y. Wu and W.-H. Zhu, Bonding strength regulates anchoring-based self-assembly monolayers for efficient and stable perovskite solar cells, *Adv. Funct. Mater.*, 2021, **31**, 2103847.

45 S. Y. Kim, S. J. Cho, S. E. Byeon, X. He and H. J. Yoon, Self-assembled monolayers as interface engineering nanomaterials in perovskite solar cells, *Adv. Energy Mater.*, 2020, **10**, 2002606.

46 E. Arkan, E. Yalcin, M. Unal, M. Z. Y. Arkan, M. Can, C. Tozlu and S. Demic, Effect of functional groups of self-assembled monolayer molecules on the performance of inverted perovskite solar cell, *Mater. Chem. Phys.*, 2020, **254**, 123435.

47 E. Arkan, M. Unal, E. Yalcin, M. Z. Yigit Arkan, S. Yurtdas, M. Can, C. Tozlu and S. Demic, Influence of end groups variation of self-assembled monolayers on performance of planar perovskite solar cells by interface regulation, *Mater. Sci. Semicond. Process.*, 2021, **123**, 105514.

48 E. Arkan, M. Z. Yigit Arkan, M. Unal, E. Yalcin, H. Aydin, C. Celebi, M. Can, C. Tozlu and S. Demic, Performance enhancement of inverted perovskite solar cells through interface engineering by TPD based bidentate self-assembled monolayers, *Opt. Mater.*, 2020, **105**, 109910.

49 E. Aktas, N. Phung, H. Köbler, D. A. González, M. Méndez, I. Kafedjiska, S.-H. Turren-Cruz, R. Wenisch, I. Lauermann, A. Abate and E. Palomares, Understanding the perovskite/self-assembled selective contact interface for ultra-stable and highly efficient p–i–n perovskite solar cells, *Energy Environ. Sci.*, 2021, **14**, 3976–3985.

50 E. Yalcin, M. Can, C. Rodriguez-Seco, E. Aktas, R. Pudi, W. Cambarau, S. Demic and E. Palomares, Conformal

monolayer contacts with lossless interfaces for perovskite single junction and monolithic tandem solar cells, *Energy Environ. Sci.*, 2019, **12**, 230–237.

51 E. Aktas, R. Pudi, N. Phung, R. Wenisch, L. Gregori, D. Meggiolaro, M. A. Flatken, F. De Angelis, I. Lauermann, A. Abate and E. Palomares, Role of terminal group position in triphenylamine-based self-assembled hole-selective molecules in perovskite solar cells, *ACS Appl. Mater. Interfaces*, 2022, **14**, 17461–17469.

52 J. Zhang, Y. Sun and H. Yu, Reducing energy loss via adjusting the anode work function and perovskite layer morphology for the efficient and stable hole transporting layer-free perovskite solar cells, *Chem. Eng. J.*, 2022, **431**, 133948.

53 W. Li, M. Cariello, M. Méndez, G. Cooke and E. Palomares, Self-assembled molecules for hole-selective electrodes in highly stable and efficient inverted perovskite solar cells with ultralow energy loss, *ACS Appl. Energy Mater.*, 2023, **6**, 1239–1247.

54 Y. Wang, Q. Liao, J. Chen, W. Huang, X. Zhuang, Y. Tang, B. Li, X. Yao, X. Feng, X. Zhang, M. Su, Z. He, T. J. Marks, A. Facchetti and X. Guo, Teaching an old anchoring group new tricks: enabling low-cost, eco-friendly hole-transporting materials for efficient and stable perovskite solar cells, *J. Am. Chem. Soc.*, 2020, **142**, 16632–16643.

55 Q. Liao, Y. Wang, Z. Zhang, K. Yang, Y. Shi, K. Feng, B. Li, J. Huang, P. Gao and X. Guo, Self-assembled donor-acceptor hole contacts for inverted perovskite solar cells with an efficiency approaching 22%: The impact of anchoring groups, *J. Energy Chem.*, 2022, **68**, 87–95.

56 Q. Liao, Y. Wang, M. Hao, B. Li, K. Yang, X. Ji, Z. Wang, K. Wang, W. Chi, X. Guo and W. Huang, Green-solvent-processable low-cost fluorinated hole contacts with optimized buried interface for highly efficient perovskite solar cells, *ACS Appl. Mater. Interfaces*, 2022, **14**, 43547–43557.

57 S. Zhang, R. Wu, C. Mu, Y. Wang, L. Han, Y. Wu and W.-H. Zhu, Conjugated self-assembled monolayer as stable hole-selective contact for inverted perovskite solar cells, *ACS Mater. Lett.*, 2022, **4**, 1976–1983.

58 S. Huang, Z. Liu, J. Xu, D. Zhang, H. Dong, Z. Wu and L. Duan, Self-assembly monomolecular engineering towards efficient and stable inverted perovskite solar cells, *Chem. Eng. J.*, 2022, **430**, 132986.

59 M. Más-Montoya, P. Gómez, D. Curiel, I. da Silva, J. Wang and R. A. J. Janssen, A Self-assembled small-molecule-based hole-transporting material for inverted perovskite solar cells, *Chem. – Eur. J.*, 2020, **26**, 10276–10282.

60 W. Kong, W. Li, C. Liu, H. Liu, J. Miao, W. Wang, S. Chen, M. Hu, D. Li, A. Amini, S. Yang, J. Wang, B. Xu and C. Cheng, Organic monomolecular layers enable energy-level matching for efficient hole transporting layer free inverted perovskite solar cells, *ACS Nano*, 2019, **13**, 1625–1634.

61 J. Cao, C.-K. Liu, V. Piradi, H.-L. Loi, T. Wang, H. Cheng, X. Zhu and F. Yan, Ultrathin self-assembly two-dimensional metal–organic framework films as hole transport layers in

ideal-bandgap perovskite solar cells, *ACS Energy Lett.*, 2022, **7**, 3362–3369.

62 C.-Y. Chang, H.-H. Huang, H. Tsai, S.-L. Lin, P.-H. Liu, W. Chen, F.-C. Hsu, W. Nie, Y.-F. Chen and L. Wang, Facile fabrication of self-assembly functionalized polythiophene hole transporting layer for high performance perovskite solar cells, *Adv. Sci.*, 2021, **8**, 2002718.

63 Z. Zhu, Y. Bai, T. Zhang, Z. Liu, X. Long, Z. Wei, Z. Wang, L. Zhang, J. Wang, F. Yan and S. Yang, High-performance hole-extraction layer of sol–gel-processed NiO nanocrystals for inverted planar perovskite solar cells, *Angew. Chem., Int. Ed.*, 2014, **53**, 12571–12575.

64 L. Xu, X. Chen, J. Jin, W. Liu, B. Dong, X. Bai, H. Song and P. Reiss, Inverted perovskite solar cells employing doped NiO hole transport layers: A review, *Nano Energy*, 2019, **63**, 103860.

65 N. Tiwari, H. Arianita Dewi, E. Erdenebileg, R. Narayan Chauhan, N. Mathews, S. Mhaisalkar and A. Bruno, Advances and potentials of NiO$_x$ surface treatments for p–i–n perovskite solar cells, *Sol. RRL*, 2022, **6**, 2100700.

66 W. Han, G. Ren, J. Liu, Z. Li, H. Bao, C. Liu and W. Guo, Recent progress of inverted perovskite solar cells with a modified PEDOT:PSS hole transport layer, *ACS Appl. Mater. Interfaces*, 2020, **12**, 49297–49322.

67 Q. Wang, C.-C. Chueh, T. Zhao, J. Cheng, M. Eslamian, W. C. H. Choy and A. K.-Y. Jen, Effects of self-assembled monolayer modification of nickel oxide nanoparticles layer on the performance and application of inverted perovskite solar cells, *ChemSusChem*, 2017, **10**, 3794–3803.

68 H. Cheng, Y. Li, G. Zhao, K. Zhao and Z.-S. Wang, Pyridine-terminated conjugated organic molecules as an interfacial hole transfer bridge for NiO$_x$-based perovskite solar cells, *ACS Appl. Mater. Interfaces*, 2019, **11**, 28960–28967.

69 Y.-W. Zhang, P.-P. Cheng, J.-M. Liang, W.-Y. Tan and Y. Min, Morphology control of the perovskite thin films via the surface modification of nickel oxide nanoparticles layer using a bidentate chelating ligand 2,2′-Bipyridine, *Synth. Met.*, 2019, **258**, 116197.

70 Y. Bai, H. Chen, S. Xiao, Q. Xue, T. Zhang, Z. Zhu, Q. Li, C. Hu, Y. Yang, Z. Hu, F. Huang, K. S. Wong, H.-L. Yip and S. Yang, Effects of a molecular monolayer modification of NiO nanocrystal layer surfaces on perovskite crystallization and interface contact toward faster hole extraction and higher photovoltaic performance, *Adv. Funct. Mater.*, 2016, **26**, 2950–2958.

71 J. Zhang, J. Yang, R. Dai, W. Sheng, Y. Su, Y. Zhong, X. Li, L. Tan and Y. Chen, Elimination of interfacial lattice mismatch and detrimental reaction by self-assembled layer dual-passivation for efficient and stable inverted perovskite solar cells, *Adv. Energy Mater.*, 2022, **12**, 2103674.

72 X. Zhu, C. F. J. Lau, K. Mo, S. Cheng, Y. Xu, R. Li, C. Wang, Q. Zheng, Y. Liu, T. Wang, Q. Lin and Z. Wang, Inverted planar heterojunction perovskite solar cells with high ultraviolet stability, *Nano Energy*, 2022, **103**, 107849.

73 M. Chen, G. Kapil, L. Wang, S. Razey Sahamir, A. K. Baranwal, K. Nishimura, Y. Sanehira, Z. Zhang, M. Akmal Kamarudin, Q. Shen and S. Hayase, High performance wide bandgap Lead-free perovskite solar cells by monolayer engineering, *Chem. Eng. J.*, 2022, **436**, 135196.

74 Z. Deng, R. Zhao, T. Guo, Z. Zhang, Y. Xing, J. Zhang, X. Liu, L. Huang, Z. Hu and Y. Zhu, Interface dipole at nickel oxide surface to enhance the photovoltage of perovskite solar cells, *Colloids Surf., A*, 2022, **652**, 129788.

75 D. S. Mann, P. Patil, S.-N. Kwon and S.-I. Na, Enhanced performance of p–i–n perovskite solar cell via defect passivation of nickel oxide/perovskite interface with self-assembled monolayer, *Appl. Surface Sci.*, 2021, **560**, 149973.

76 P. Topolovsek, F. Lamberti, T. Gatti, A. Cito, J. M. Ball, E. Menna, C. Gadermaier and A. Petrozza, Functionalization of transparent conductive oxide electrode for TiO$_2$-free perovskite solar cells, *J. Mater. Chem. A*, 2017, **5**, 11882–11893.

77 H. Cheng, Y. Li, M. Zhang, K. Zhao and Z.-S. Wang, Self-assembled ionic liquid for highly efficient electron transport layer-free perovskite solar cells, *ChemSusChem*, 2020, **13**, 2779–2785.

78 L. Li, Y. Wu, E. Li, C. Shen, H. Zhang, X. Xu, G. Wu, M. Cai and W.-H. Zhu, Self-assembled naphthalimide derivatives as an efficient and low-cost electron extraction layer for n–i–p perovskite solar cells, *Chem. Commun.*, 2019, **55**, 13239–13242.

79 F. Ye, D. Zhang, X. Xu, H. Guo, S. Liu, S. Zhang, Y. Wu and W.-H. Zhu, Anchorable perylene diimides as chemically inert electron transport layer for efficient and stable perovskite solar cells with high reproducibility, *Sol. RRL*, 2021, **5**, 2000736.

80 S. O. Fürer, K. J. Rietwyk, F. Pulvirenti, D. P. McMeekin, M. A. Surmiak, S. R. Raga, W. Mao, X. Lin, Y. Hora, J. Wang, Y. Shi, S. Barlow, D. S. Ginger, S. R. Marder and U. Bach, Naphthalene-imide self-assembled monolayers as a surface modification of ITO for improved thermal stability of perovskite solar cells, *ACS Appl. Energy Mater.*, 2023, **6**, 667–677.

81 H. Zhou, Q. Chen, G. Li, S. Luo, T.-B. Song, H.-S. Duan, Z. Hong, J. You, Y. Liu and Y. Yang, Interface engineering of highly efficient perovskite solar cells, *Science*, 2014, **345**, 542–546.

82 H. Tan, A. Jain, O. Voznyy, X. Lan, F. P. García de Arquer, J. Z. Fan, R. Quintero-Bermudez, M. Yuan, B. Zhang, Y. Zhao, F. Fan, P. Li, L. N. Quan, Y. Zhao, Z.-H. Lu, Z. Yang, S. Hoogland and E. H. Sargent, Efficient and stable solution-processed planar perovskite solar cells via contact passivation, *Science*, 2017, **355**, 722–726.

83 Y. Ding, B. Ding, H. Kanda, O. J. Usiobo, T. Gallet, Z. Yang, Y. Liu, H. Huang, J. Sheng, C. Liu, Y. Yang, V. I. E. Queloz, X. Zhang, J.-N. Audinot, A. Redinger, W. Dang, E. Mosconic, W. Luo, F. De Angelis, M. Wang, P. Dörflinger, M. Armer, V. Schmid, R. Wang, K. G. Brooks, J. Wu, V. Dyakonov, G. Yang, S. Dai, P. J. Dyson and M. K. Nazeeruddin, Single-crystalline TiO$_2$ nanoparticles for stable and efficient perovskite modules, *Nat. Nanotechnol.*, 2022, **17**, 598–605.

84 K. Wojciechowski, S. D. Stranks, A. Abate, G. Sadoughi, A. Sadhanala, N. Kopidakis, G. Rumbles, C.-Z. Li, R. H. Friend, A. K. Y. Jen and H. J. Snaith, Heterojunction modification for highly efficient organic–inorganic perovskite solar cells, *ACS Nano*, 2014, **8**, 12701–12709.

85 A. Abrusci, S. D. Stranks, P. Docampo, H.-L. Yip, A. K. Y. Jen and H. J. Snaith, High-performance perovskite-polymer hybrid solar cells via electronic coupling with fullerene monolayers, *Nano Lett.*, 2013, **13**, 3124–3128.

86 Y. Ogomi, A. Morita, S. Tsukamoto, T. Saitho, Q. Shen, T. Toyoda, K. Yoshino, S. S. Pandey, T. Ma and S. Hayase, All-solid perovskite solar cells with HOCO-R-NH$_3^+$I$^-$ anchor-group inserted between porous titania and perovskite, *J. Phys. Chem. C*, 2014, **118**, 16651–16659.

87 L. Liu, A. Mei, T. Liu, P. Jiang, Y. Sheng, L. Zhang and H. Han, Fully printable mesoscopic perovskite solar cells with organic silane self-assembled monolayer, *J. Am. Chem. Soc.*, 2015, **137**, 1790–1793.

88 Z. Chen, Y. Li, Z. Liu, J. Shi, B. Yu, S. Tan, Y. Cui, C. Tan, F. Tian, H. Wu, Y. Luo, D. Li and Q. Meng, Reconfiguration toward self-assembled monolayer passivation for high-performance perovskite solar cells, *Adv. Energy Mater.*, 2022, 2202799.

89 T. Zhu, J. Su, F. Labat, I. Ciofini and T. Pauporté, Interfacial engineering through chloride-functionalized self-assembled monolayers for high-performance perovskite solar cells, *ACS Appl. Mater. Interfaces*, 2020, **12**, 744–752.

90 F. Han, G. Hao, Z. Wan, J. Luo, J. Xia and C. Jia, Bifunctional electron transporting layer/perovskite interface linker for highly efficient perovskite solar cells, *Electrochim. Acta*, 2019, **296**, 75–81.

91 J. Cao, J. Yin, S. Yuan, Y. Zhao, J. Li and N. Zheng, Thiols as interfacial modifiers to enhance the performance and stability of perovskite solar cells, *Nanoscale*, 2015, **7**, 9443–9447.

92 S. Y. Abate, D.-C. Huang and Y.-T. Tao, Surface modification of TiO$_2$ layer with phosphonic acid monolayer in perovskite solar cells: Effect of chain length and terminal functional group, *Org. Electron.*, 2020, **78**, 105583.

93 Q. Jiang, L. Zhang, H. Wang, X. Yang, J. Meng, H. Liu, Z. Yin, J. Wu, X. Zhang and J. You, Enhanced electron extraction using SnO$_2$ for high-efficiency planar-structure HC(NH$_2$)$_2$PbI$_3$-based perovskite solar cells, *Nat. Energy*, 2016, **2**, 16177.

94 Q. Jiang, X. Zhang and J. You, SnO$_2$: A wonderful electron transport layer for perovskite solar cells, *Small*, 2018, **14**, 1801154.

95 Z. Dai, S. K. Yadavalli, M. Chen, A. Abbaspourtamijani, Y. Qi and N. P. Padture, Interfacial toughening with self-assembled monolayers enhances perovskite solar cell reliability, *Science*, 2021, **372**, 618–622.

96 Z. Wang, M. A. Kamarudin, N. C. Huey, F. Yang, M. Pandey, G. Kapil, T. Ma and S. Hayase, Interfacial sulfur functionalization anchoring SnO$_2$ and CH$_3$NH$_3$PbI$_3$ for enhanced stability and trap passivation in perovskite solar cells, *ChemSusChem*, 2018, **11**, 3941–3948.

97 L. Zuo, Q. Chen, N. De Marco, Y.-T. Hsieh, H. Chen, P. Sun, S.-Y. Chang, H. Zhao, S. Dong and Y. Yang, Tailoring the interfacial chemical interaction for high-efficiency perovskite solar cells, *Nano Lett.*, 2017, **17**, 269–275.

98 X. Zuo, B. Kim, B. Liu, L. He, L. Bai, W. Wang, C. Xu, Q. Song, C. Jia, Z. Zang, D. Lee, X. Li and J. Chen, Passivating buried interface via self-assembled novel sulfonium salt toward stable and efficient perovskite solar cells, *Chem. Eng. J.*, 2022, **431**, 133209.

99 J. Du, L. Feng, X. Guo, X. Huang, Z. Lin, J. Su, Z. Hu, J. Zhang, J. Chang and Y. Hao, Enhanced efficiency and stability of planar perovskite solar cells by introducing amino acid to SnO$_2$/perovskite interface, *J. Power Sources*, 2020, **455**, 227974.

100 X. Sun, H. Jiang, Y. Sun, Z. Guo, Z. Pang, F. Wang, J. Yang and L. Yang, Multi-functional L-histidine self-assembled monolayers on SnO$_2$ electron transport layer to boost photovoltaic performance of perovskite solar cells, *Electrochim. Acta*, 2022, **428**, 140930.

101 M. Hou, H. Zhang, Z. Wang, Y. Xia, Y. Chen and W. Huang, Enhancing efficiency and stability of perovskite solar cells via a self-assembled dopamine interfacial layer, *ACS Appl. Mater. Interfaces*, 2018, **10**, 30607–30613.

102 Y. Shi, H. Zhang, X. Tong, X. Hou, F. Li, Y. Du, S. Wang, Q. Zhang, P. Liu and X. Zhao, Interfacial engineering via self-assembled thiol silane for high efficiency and stability perovskite solar cells, *Sol. RRL*, 2021, **5**, 2100128.

103 K. Liu, S. Chen, J. Wu, H. Zhang, M. Qin, X. Lu, Y. Tu, Q. Meng and X. Zhan, Fullerene derivative anchored SnO$_2$ for high-performance perovskite solar cells, *Energy Environ. Sci.*, 2018, **11**, 3463–3471.

104 P. Zhang, J. Wu, T. Zhang, Y. Wang, D. Liu, H. Chen, L. Ji, C. Liu, W. Ahmad, Z. D. Chen and S. Li, Perovskite solar cells with ZnO electron-transporting materials, *Adv. Mater.*, 2018, **30**, 1703737.

105 J. Cao, B. Wu, R. Chen, Y. Wu, Y. Hui, B.-W. Mao and N. Zheng, Efficient, hysteresis-free, and stable perovskite solar cells with ZnO as electron-transport layer: effect of surface passivation, *Adv. Mater.*, 2018, **30**, 1705596.

106 J. Yang, B. D. Siempelkamp, E. Mosconi, F. De Angelis and T. L. Kelly, Origin of the thermal instability in CH$_3$NH$_3$PbI$_3$ thin films deposited on ZnO, *Chem. Mater.*, 2015, **27**, 4229–4236.

107 Q. An, P. Fassl, Y. J. Hofstetter, D. Becker-Koch, A. Bausch, P. E. Hopkinson and Y. Vaynzof, High performance planar perovskite solar cells by ZnO electron transport layer engineering, *Nano Energy*, 2017, **39**, 400–408.

108 L. Zuo, Z. Gu, T. Ye, W. Fu, G. Wu, H. Li and H. Chen, Enhanced photovoltaic performance of CH$_3$NH$_3$PbI$_3$ perovskite solar cells through interfacial engineering using self-assembling monolayer, *J. Am. Chem. Soc.*, 2015, **137**, 2674–2679.

109 J. Han, H. Kwon, E. Kim, D.-W. Kim, H. J. Son and D. H. Kim, Interfacial engineering of a ZnO electron transporting layer using self-assembled monolayers for high performance and stable perovskite solar cells, *J. Mater. Chem. A*, 2020, **8**, 2105–2113.

110 R. Azmi, W. T. Hadmojo, S. Sinaga, C.-L. Lee, S. C. Yoon, I. H. Jung and S.-Y. Jang, High-efficiency low-temperature ZnO based perovskite solar cells based on highly polar, nonwetting self-assembled molecular layers, *Adv. Energy Mater.*, 2018, **8**, 1701683.

111 C. M. Wolff, L. Canil, C. Rehermann, N. Ngoc Linh, F. Zu, M. Ralaiarisoa, P. Caprioglio, L. Fiedler, M. Stolterfoht, S. Kogikoski, Jr., I. Bald, N. Koch, E. L. Unger, T. Dittrich, A. Abate and D. Neher, Perfluorinated self-assembled monolayers enhance the stability and efficiency of inverted perovskite solar cells, *ACS Nano*, 2020, **14**, 1445–1456.

112 Y. Bai, Q. Dong, Y. Shao, Y. Deng, Q. Wang, L. Shen, D. Wang, W. Wei and J. Huang, Enhancing stability and efficiency of perovskite solar cells with crosslinkable silane-functionalized and doped fullerene, *Nat. Commun.*, 2016, **7**, 12806.

113 H. Guo, Y. Fang, H.-B. Cheng, J. Wu, Y. Lei, S. Wang, X. Li, Y. Dai, W. Xiang, D.-J. Xue, Y. Lin and A. Hagfeldt, Robust self-assembled molecular passivation for high-performance perovskite solar cells, *Angew. Chem., Int. Ed.*, 2022, **61**, e202204148.

114 J. Zhang, Z. Hu, L. Huang, G. Yue, J. Liu, X. Lu, Z. Hu, M. Shang, L. Han and Y. Zhu, Bifunctional alkyl chain barriers for efficient perovskite solar cells, *Chem. Commun.*, 2015, **51**, 7047–7050.

115 G. Wang, C. Wang, Y. Gao, S. Wen, R. C. I. MacKenzie, L. Guo, W. Dong and S. Ruan, Passivation agent with dipole moment for surface modification towards efficient and stable perovskite solar cells, *J. Energy Chem.*, 2022, **64**, 55–61.

116 H. Zhong, Z. Jia, J. Shen, Z. Yu, S. Yin, X. Liu, G. Fu, S. Chen, S. Yang and W. Kong, Surface treatment of the perovskite via self-assembled dipole layer enabling enhanced efficiency and stability for perovskite solar cells, *Appl. Surf. Sci.*, 2022, **602**, 154365.

117 T. Wu, Y. Wang, X. Li, Y. Wu, X. Meng, D. Cui, X. Yang and L. Han, Efficient Defect Passivation for Perovskite Solar Cells by Controlling the Electron Density Distribution of Donor-π-Acceptor Molecules, *Adv. Energy Mater.*, 2019, **9**, 1803766.

118 C. Zhang, W. Kong, T. Wu, X. Lin, Y. Wu, J. Nakazaki, H. Segawa, X. Yang, Y. Zhang, Y. Wang and L. Han, Reduction of Nonradiative Loss in Inverted Perovskite Solar Cells by Donor−π−Acceptor Dipoles, *ACS Appl. Mater. Interfaces*, 2021, **13**, 44321–44328.

119 J. Dagar, M. Fenske, A. Al-Ashouri, C. Schultz, B. Li, H. Köbler, R. Munir, G. Parmasivam, J. Li, I. Levine, A. Merdasa, L. Kegelmann, H. Näsström, J. A. Marquez, T. Unold, D. M. Többens, R. Schlatmann, B. Stegemann, A. Abate, S. Albrecht and E. Unger, Compositional and interfacial engineering yield high-performance and stable p–i–n perovskite solar cells and mini-modules, *ACS Appl. Mater. Interfaces*, 2021, **13**, 13022–13033.

120 J. Zeng, L. Bi, Y. Cheng, B. Xu and A. K. Y. Jen, Self-assembled monolayer enabling improved buried interfaces in blade-coated perovskite solar cells for high efficiency and stability, *Nano Res. Energy*, 2022, **1**, e9120004.

121 E. Li, E. Bi, Y. Wu, W. Zhang, L. Li, H. Chen, L. Han, H. Tian and W.-H. Zhu, Synergistic co-assembly of highly wettable and uniform hole-extraction monolayers for scaling-up perovskite solar cells, *Adv. Funct. Mater.*, 2020, **30**, 1909509.

122 Z. Gu, L. Zuo, T. T. Larsen-Olsen, T. Ye, G. Wu, F. C. Krebs and H. Chen, Interfacial engineering of self-assembled monolayer modified semi-roll-to-roll planar heterojunction perovskite solar cells on flexible substrates, *J. Mater. Chem. A*, 2015, **3**, 24254–24260.